The most primitive CM chondrites, Asuka 12085, 12169, and 12236, of subtypes 3.0–2.8: Their characteristic features and classification

Journal Item

The most primitive CM chondrites, Asuka 12085, 12169, and 12236, of subtypes 3.0–2.8: Their characteristic features and classification

M. Kimura, N. Imae, M. Komatsu, J.A. Barrat, R.C. Greenwood, A. Yamaguchi, T. Noguchi

PII: S1873-9652(20)30074-8

DOI: https://doi.org/10.1016/j.polar.2020.100565

Reference: POLAR 100565

To appear in: *Polar Science*

Received Date: 19 April 2020

Revised Date: 26 July 2020

Accepted Date: 6 August 2020

Please cite this article as: Kimura, M., Imae, N., Komatsu, M., Barrat, J.A., Greenwood, R.C., Yamaguchi, A., Noguchi, T., The most primitive CM chondrites, Asuka 12085, 12169, and 12236, of subtypes 3.0–2.8: Their characteristic features and classification, *Polar Science* (2020), doi: https://doi.org/10.1016/j.polar.2020.100565.

The most primitive CM chondrites, Asuka 12085, 12169, and 12236, of subtypes 3.0-2.8: Their characteristic features and classification

M. Kimura[1,*], N. Imae[1], M. Komatsu[2], J. A. Barrat[3], R. C. Greenwood[4], A. Yamaguchi[1], and T. Noguchi[5]

[1]National Institute of Polar Research, Tokyo 190-8518, Japan, [2]SOKENDAI, Kanagawa 240-0193, Japan, [3]Université de Bretagne Occidentale, Institut Universitaire Europé en de la Mer, CNRS UMR 6538, Place Nicolas Copernic, 29280 Plouzané, France, [4]Planetary and Space Sciences, The Open University, Milton Keynes MK7 6AA, United Kingdom, [5]Kyushu University, Fukuoka 819-0395, Japan.

* Corresponding author, kimura.makoto@nipr.ac.jp

Abstract

CM chondrites (CMs) are the most abundant group of carbonaceous chondrites. CMs experienced varying degrees of secondary aqueous alteration and heating that modified or destroyed their primitive features. We have studied three chondrites, Asuka (A) 12085, A 12169, and A 12236. Their modal compositions, chondrule size distributions, and bulk composition indicate that they are CMs. However, the common occurrence of melilite in CAIs and glass in chondrules, abundant Fe-Ni metal, the absence of tochilinite-cronstedtite intergrowths, and almost no phyllosilicates, all suggest that these chondrites, especially A 12169, experienced only minimal aqueous alteration. The textures and compositions of metal and sulfides, the lack of ferroan rims on AOA olivines, the compositional distribution of ferroan olivine, and the Raman spectra of their matrices, indicate that these chondrites experienced neither significant heating nor dehydration.

These chondrites, especially A 12169, are the most primitive CMs so far reported. The degree of the alteration increases from A 12169, through A 12236, to A 12085. We propose the criteria for subtypes of 3.0-2.8 for CMs. A 12169, A 12236, and A 12085 are classified as subtype 3.0, 2.9, and 2.8, respectively. The oxygen isotopic composition of the Asuka CMs is consistent with these samples having experienced only a limited degree of aqueous alteration. The CM and CO groups are probably not derived from a single heterogeneous parent body. These chondrites are also of particular significance in view of the imminent return of sample material from the asteroids Ryugu and Bennu.

Keywords: Meteorites, Carbonaceous chondrite, Classification, Oxygen isotopes, CM2 CO3 precursors

1. Introduction

Carbonaceous (C) chondrites are some of the most primitive materials in the solar system, and are classified into eight major chemical groups, CI, CM, CO, CV, CR, CH, CB, and CK (e.g., Weisberg et al., 2006). The CMs are the most abundant group of C chondrites (after Krot et al., 2014) and appear to be widely distributed within the inner solar system, occurring as brecciated fragments and clasts in a wide range of meteorite types (e.g., Zolensky et al., 1996).

All known CMs have lost their primitive features because of aqueous alteration and/or secondary heating (e.g., Rubin et al., 2007; Nakamura, 2005), with the notable exception of the CMs that are the focus of this work, based on the preliminary results of Kimura et al. (2019). Some weakly altered CM and related chondrites have been recently reported, such as Paris (Hewins et al.,

2014), EET 96029 (Lee et al., 2016), NWA 5958 (Jacquet et al., 2016), LEW 85311 (Lee et al., 2019), and NWA 11024 (Ebert et al., 2019). However, their primitive features before alteration are not completely preserved in them. Recently, Yamaguchi et al. (2016) reported the recovery of three CMs, Asuka (A) 12085, A 12169, and A 12236. Here we report the petrography, mineralogy, bulk chemistry and oxygen isotope composition of these chondrites, to explore their characteristic features, classifications, and precursor materials.

We will conclude that these three Asuka chondrites are CMs and that they are amongst the most primitive members of this group so far reported. These chondrites provide important information about the primitive features of CMs before the secondary processes in their parent body. We propose subtypes 3.0-2.8 for CMs, modified from Rubin (2015).

2. Samples and experimental methods

The joint expedition party between Japan and Belgium (JARE-54 and BELARE 2012-2013) collected 420 meteorites from the Nansen Ice Field, Antarctica (Imae et al., 2015). A 12085, A 12169, and A 12236 are included in this collection and were recovered in a 7km x 2km area of the area B (Imae et al., 2015). The original (recovered) weights of A 12085, A 12169, and A 12236 were 9.114, 2.264, 93.65 g, respectively. For this study, we have examined the polished thin sections, A 12085,41-1, A 12169,31-1, and A 12236,51-1. The area of theses sections are 151.9, 42.0 and 98.1 mm^2, respectively.

In order to compare these chondrites with the other C chondrites, we also analyzed A 12248 (CM2.0), Murchison (CM2.5), ALH-77307 (CO3.03), and Y-81020 (CO3.05).

Back-scattered electron (BSE) images were obtained using the JEOL JSM-7100F field emission scanning electron microscope (FESEM) at the National Institute of Polar Research

(NIPR). We conducted mineral analyses using the JEOL JXA8200 electron-probe microanalyzer at NIPR, with a focused beam, and 10-30 nA beam currents for silicate phases and 30 nA beam current for opaque minerals. All these analytical methods have been previously described by Yamaguchi et al. (2011). The matrix was measured by using a defocused beam (5 µm in diameter) for ~100-200 randomly selected points that avoided coarse-grained silicate and opaque minerals to calculate an average bulk matrix composition. The elemental X-ray maps of the whole thin sections were obtained using the FESEM. We obtained the modal compositions of the sections from the elemental maps, using ImageJ software.

We identified some phases using a laser micro Raman spectrometer (JASCO NRS-1000) using 532-nm excitation at the NIPR, after the method of Kimura et al. (2017). Raman spectra for D- and G-bands were also collected on randomly-selected matrix areas on the sections after the method of Komatsu et al. (2018). Imae et al. (2019) have recently applied an X-ray diffraction (XRD) method to characterize minerals in meteorite thin sections by using SmartLab, RIGAKU at the NIPR. We used the same method for the samples studied here, although the silicon 100 index wafer with the opening 8 mm in diameter and the 125 µm thickness was used in this study, to reduce the diffraction from epoxy resin surrounding the sample. The accuracy of the diffraction angle is within 0.02º. Isolated peaks for a phase were used, which do not overlap with the other phases. We use only intense peaks for phase identification, and they are normally 1000-10000 counts much higher than the background level. We did not use the other lower peaks because of the ambiguous identification of peaks.

Trace elements for A 12236, the largest among samples studied here, were determined by ICP-SFMS and ICP-AES using the same procedure as Barrat et al. (2012) and Kimura et al. (2014).

The bulk oxygen isotope compositions of A 12085, A 12169 and A 12236 were determined by infrared laser-assisted fluorination at the Open University (Miller et al., 1999; Greenwood et al., 2017). Whole-rock powders of the three CMs were prepared by crushing and homogenizing approximately 100 mg fresh interior chips for each of the samples.

Due to their relatively high phyllosilicate contents, CM chondrites can be challenging samples to analyse by laser fluorination. This is essentially because the normal blank reduction procedure, which involves flushing the chamber with aliquots of BrF_5, may lead to the preferential reduction of the hydrated silicate fraction prior to analysis. To minimise this problem, A 12085, A 12169 and A 12236 were all run in "single shot" mode, with only one standard and one 2 mg sample aliquot loaded in the sample chamber at a time. Further details of the "single shot" procedure are given in Lee et al. (2019).

Analytical precision (2σ) for the Open University system, based on replicate analyses of an internal obsidian standard, is ±0.053‰ for $\delta^{17}O$; ±0.095‰ for $\delta^{18}O$; ±0.018‰ for $\Delta^{17}O$ (2σ) (Starkey et al., 2016). Oxygen isotopic analysis for the three CMs are reported in standard δ notation, where $\delta^{18}O$ has been calculated as: $\delta^{18}O = [(^{18}O/^{16}O)_{sample}/(^{18}O/^{16}O)_{ref} - 1] \times 1000$ (‰) and similarly for $\delta^{17}O$ using the $^{17}O/^{16}O$ ratio, the reference being VSMOW: Vienna Standard Mean Ocean Water. For the purposes of comparison with the results of Clayton and Mayeda (1999) $\Delta^{17}O$, which represents the deviation from the terrestrial fractionation line, has been calculated as: $\Delta^{17}O = \delta^{17}O - 0.52 \times \delta^{18}O$.

3. Results

3.1 Petrography

3.1.1 Overall features and modal compositions

A 12085, A 12169, and A 12236 show typical C chondritic textures, mainly consisting of chondrules, refractory inclusions, isolated silicates and opaque minerals, and matrix (Fig. 1). None of these chondrites show brecciated textures, but some clasts are encountered in A 12085 and 12169. Figure 1c shows that Ca-Al-rich inclusions (CAIs) are common in A 12169.

Table 1 compares the modal abundances of the Asuka chondrites with weakly altered CMs whose detailed modal data are known. The most abundant component is the matrix, followed by chondrules in the Asuka chondrites (Table 1). The modal abundances of chondrules with isolated silicate minerals are 29 - 39 vol. % and those of matrices are 53 - 65 %. They are within the ranges for CMs (Weisberg et al., 2006). The abundances of refractory inclusions are 3.8 - 4.3 vol.%. One of the distinct features of these chondrites is the abundant occurrence of Fe-Ni metal, 1.2 - 2.3 vol.% (Table 1). The abundances of metal are much higher than those (<1.2 vol.%) in CM2.7-2.0 (Rubin et al., 2007; Rubin, 2015). Sulfide minerals are also abundant, 0.9-1.4 vol.%, in these chondrites.

These chondrites have experienced only very low levels of shock metamorphism (shock stage 1) or terrestrial weathering (A) (Yamaguchi et al., 2016). A 12169 section has fusion crusts (below ~1.5 mm in width).

3.1.2 Refractory inclusions

Refractory inclusions are easily recognizable in these chondrites. The sizes of the refractory inclusions are smaller than ~300 μm. Many CAIs are surrounded by rims, consisting mainly of high-Ca pyroxene (Fig. 2a). The CAIs commonly consist of spinel, melilite, and high-Ca pyroxene, with a minor amount of perovskite and grossite. Melilite is abundant in the CAIs. Melilite-bearing CAIs are 70, 60, and 20% of all CAIs in A 12169, A 12236, and A 12085, respectively, although

spinel-pyroxene CAIs are predominant in A 12085. Secondary alteration minerals, such as phyllosilicate, nepheline, sodalite, and hedenbergite, are not encountered in these CAIs.

Amoeboid olivine aggregates (AOAs) are also common in these chondrites. The AOAs mostly consist of forsteritic olivine, with minor amounts of spinel, anorthite and high-Ca pyroxene intergrown with olivine grains (Fig. 2b). The AOA olivines do not have visible FeO-rich rims. AOAs in these meteorites do not contain any secondary minerals, as was also the case for the CAIs.

3.1.3 Chondrules and isolated silicate minerals

Sharply delineated chondrules are an abundant component in these chondrites (Fig. 2c). Table 2 summarizes the characteristic features of the chondrules. Their apparent average diameter, ~0.3 mm, is typical of CMs (Weisberg et al., 2006).

Porphyritic chondrules are the most common type, with a few barred chondrules also present (Table 2). The abundances of radial and cryptocrystalline chondrules are below 3%. Type I chondrules, ~90 % of all chondrules, are much more abundant than type II. The relatively high abundance of type I, compared to type II chondrules, is a characteristic feature of CM chondrites. Most porphyritic chondrules, especially type Is, consist of olivine and low-Ca pyroxene, with minor amounts of high-Ca pyroxene, feldspar, and a spinel group mineral. Olivine, low-Ca pyroxene, and often high-Ca pyroxene are phenocryst phases in chondrules (Fig. 2d). Low-Ca pyroxene is identified as clinoenstatite, based on optical microscopic observations. Feldspar is an abundant mesostasis phase (Fig. 2c) and does not always show a devitrified texture when intergrown with high-Ca pyroxene. Porphyritic chondrules also contain a glassy mesostasis, especially in some of the chondrules of A 12169 (Fig. 2d). Feldspar and glass are the primary

mesostasis phases, like those in type 3 chondrites. The secondary anhydrous phases, such as nepheline and hedenbergite, found in the other C chondrites (e.g., Kimura and Ikeda, 1995), are not encountered. Type II chondrules contain abundant ferroan olivine, often with forsteritic olivine relicts (Fig. 2e). Chondrules, especially in A 12085 and A 12236, are commonly surrounded by fine-grained rims (Fig. 2e).

Olivine and pyroxene grains in chondrules do not display secondary diffusional zoning nor the phyllosilicate veinlets that are common in the more altered CMs (Lee and Lindgren, 2016). Clinoenstatite grains do not show alteration features along their twin boundaries. Tochilinite-cronstedtite intergrowths (TCI) do not present in the chondrules of these meteorites, in clear contrast to most other CMs.

Phyllosilicates are sometimes encountered within the outer margins of some A 12169 chondrules, whereas they commonly occur throughout the chondrules in A 12085 (Fig. 2f). A 12236 shows features that are intermediate between A 12169 and A 12085. On the other hand, primary mesostasis, unaltered feldspar and glass are commonly present in A 12169 chondrules. These phases are also present in some chondrules from A 12236, but are uncommon in A 12085. We examined 50 chondrules selected from each chondrite, and divided them into chondrules with completely altered (no primary mesostasis), partly altered, and unaltered mesostasis (only primary mesostasis). The abundances of unaltered mesostasis-bearing chondrules decreases from A 12169, through A 12236, to A 12085 (Table 2).

Chondrules commonly contain Fe-Ni metal spherules which are usually kamacite as mentioned later. They occur within and at the outer margins of chondrules. These metals are mostly homogeneous in texture (Fig. 2g). Plessitic intergrowth, noticed in Semarkona (LL3.01) (Kimura et al., 2008), is not present.

In addition to chondrules, isolated silicate grains, less than several tens microns in size, are abundantly encountered in the matrices. They are mostly fragmental in shape and are predominantly olivine and low-Ca pyroxene. They are also unaltered. Their mineralogy, composition and fragmental morphology indicates that most of these grains were derived by disaggregation and disruption of chondrules.

3.1.4 Matrix

Figure 2h shows a matrix area of A 12169. The matrix mostly consists of fine-grained silicate phases of submicron size. Fe-Ni metal and Fe-sulfides, less than 150 μm in size, occur as isolated grains in the matrix. The Fe-sulfides are mostly troilite. Rare pentlandite is always present in association with isolated pyrrhotite grains (Fig. 2i). In addition to these larger-sized opaque minerals, fine-grained opaque minerals, submicron in size, are abundantly mixed with silicate phases in the matrix (Fig. 2h).

No TCI was observed in the matrices of these chondrites. However, aggregates of Fe-sulfide(s) mixed with silicate phases of submicron size (Fig. 2j) are present, especially in A 12085. They are not common in A 12169.

3.2 Mineralogy

3.2.1 Olivine

Table 3 shows selected analyses of silicate and oxide phases. Olivine is common in chondrules, in matrix as isolated grains, and in AOAs. Olivine in type I and II chondrules is $Fo_{92\text{-}100}$ and $Fo_{30\text{-}88}$, respectively, although some type II chondrules contain relict forsterite grains ($Fo_{<99}$). Olivines in chondrules contain <0.69 wt.% Cr_2O_3, <0.68 wt.% MnO, and <0.70 wt.% CaO.

Olivines in AOAs are Fo_{98-100}. Chemical zoning has not been observed in these AOAs. The olivines in AOAs contain <0.46 wt.% Cr_2O_3, <0.61 wt.% MnO, and <0.35 wt.% CaO.

Figure 3a shows the distribution of Fe and Mn in olivines in chondrules, isolated grains, and AOAs, including those in Murchison (CM2.5). All these chondrites show similar distributions. This Fe-Mn distribution trend is consistent with those of ferroan olivines in CM and CO chondrites (Schrader and Davidson, 2017). Olivines in some AOAs and isolated minerals show a high Mn/Fe distribution trend. Such a trend is commonly observed in AOAs (e.g., Komatsu et al., 2015).

The average Cr_2O_3 content and standard deviation for cores of ferroan olivine grains (>2 wt.% FeO) are 0.34 wt.% and 0.08, 0.35 wt.% and 0.08, and 0.32 wt.% and 0.08 for A 12085, A 12169, and A 12236, respectively. These data plot within the range of those in primitive COs and some CMs (Grossman and Brearley, 2005; Schrader and Davidson, 2017) (Fig. 3b).

3.2.2 Pyroxene

Pyroxene is the second most abundant mineral in these chondrites. It is divided into low-Ca (<0.15 atomic Ca/(Ca+Mg+Fe) ratio) and high-Ca pyroxenes. Low-Ca pyroxenes are abundant in type I chondrules and are magnesian ($En_{85-99}Fs_{0.4-9.9}Wo_{0.3-13.1}$). On the other hand, low-Ca pyroxenes are minor in type II chondrules and are ferroan ($En_{38-71}Fs_{22-61}Wo_{0.1-10.1}$). In some chondrules, Al-rich low-Ca pyroxene occurs (<14.6 wt.% Al_2O_3). Such pyroxene compositions have been reported from some other chondrites, such as Semarkona (LL) (Rubin, 2004) and Y-82094 (ungrouped C chondrite) (Kimura et al., 2014).

High-Ca pyroxenes are present in chondrules as a mesostasis phase and also as phenocrysts in both chondrules and refractory inclusions. In chondrules, the high-Ca pyroxene compositional range is $En_{48-83}Fs_{0.5-9.7}Wo_{16-46}$ in type Is and $En_{20-54}Fs_{11-56}Wo_{19-50}$ in type IIs. High-Ca pyroxenes

231 in refractory inclusions contain 0.8-38 wt.% Al_2O_3, and <5.1 wt.%TiO_2 (Table 3). A pyroxene that
232 is highly enriched in Al_2O_3, 38 wt.%, in a CAI is kushiroite (Kimura et al., 2009).
233
234 3.2.3 Feldspar and glass
235 Chondrules contain abundant feldspar or glass in their mesostasis. Feldspars are anorthositic
236 (An_{89-100}) in type I chondrules, whereas type II chondrules contain albitic feldspar (Ab_{54-77}). Cation
237 total of anorthitic feldspar ranges from 4.93-5.01, suggesting that some feldspar contain excess
238 silica component, which is reported from primitive C chondrites (e.g., Tenner et al., 2018).
239 Feldspars in refractory inclusions are always nearly pure anorthosite (An_{99-100}).
240 Chondrule glasses are enriched in feldspathic components (Fig. 4) and contain 10-33 wt.%
241 Al_2O_3, 1.9-31 wt.% CaO, and 0.2-7.2 wt.% Na_2O. The compositions resemble those of CO
242 chondrules. The total weight percent ranges from 98.1 to 101.7, suggesting that they are not
243 phyllosilicate. The occurrence of glass has been reported only in some CMs (e.g., Ikeda, 1983;
244 Hewins et al., 2014).
245
246 3.2.4 Phyllosilicates in chondrules
247 Mesostasis in chondrules also contains phyllosilicate, and their abundance depends on the
248 chondrite as mentioned before. The average analytical total of phyllosilicate-dominated areas is
249 85.5 wt.%, which is much lower than that of matrix as mentioned later. Such total weight percent
250 supports that they are phyllosilicates. Their compositions suggest that they are mixtures of
251 serpentine and saponite (Fig. 4), and similar to those in other CMs, such as Murchison, and COs
252 (this work; Ikeda, 1983).
253

254 3.2.5 Other minor minerals

255 Melilite in refractory inclusions is enriched in the gehlenite component (Geh_{77-99}). Spinel in
256 inclusions is nearly pure $MgAl_2O_4$, containing only small amounts of FeO (<0.4 wt.%) and Cr_2O_3
257 (<0.7 wt.%). Type I chondrules occasionally contain Mg-Al spinel (50-71 wt.% Al_2O_3 and 0.4-5%
258 FeO wt.%), and type II chondrules contain chromite (30-55 wt.% Cr_2O_3 and 18-28 wt.% FeO).
259 Type II chondrules contain rare phosphates, most of which are no more than a few microns in
260 diameter. One of these was identified as merrillite from the composition (Table 3). Ca-carbonate is
261 observed in a few chondrules of A 12085. Small Ca-carbonate grains were also observed in a clast
262 in A 12169. Framboidal magnetite occurs in a clast in A 12085.
263
264 3.2.6 Fe-Ni metal and sulfides

265 Table 4 gives representative compositions of Fe-Ni metal and sulfides. Fe-Ni metal is divided
266 into kamacite (<7.5 wt.% Ni) and Ni-rich metal (Kimura et al., 2008). Kamacite and Ni-rich metal
267 contain <0.6 wt.% and 0.2-2.5 wt.% Co, and 0.3-7.4 wt.% and 7.5-46.5 wt.% Ni, respectively.
268 Ni-depleted metal (0.3 wt.% Ni) was found within dusty olivines in a chondrule in A 12085. From
269 the occurrence and composition, this metal seems to be a reduction product (Leroux et al., 2003).
270 Fe-Ni metal contains <1.0 wt.% Si, <2.6 wt.% P, and <1.5 wt.% Cr, which is consistent with other
271 CMs that have experienced low degrees of heating (Kimura et al., 2011). A few grains are rich in P
272 (1.9-2.6 wt.%), but phosphides do not appear to be present. A positive correlation exists between
273 Ni and Co abundances measured in metal grains present within the matrices of these meteorites
274 (Fig. 5). Such a trend was also found in other unheated CMs and the ungrouped chondrite Acfer
275 094 (Kimura et al., 2008).

Troilite, pyrrhotite, and pentlandite were observed in these three chondrites. Pyrrhotite and pentlandite contain 0.2-2.9 wt.% Ni and <0.3 wt.% Co, and 16-34 wt.% and 0.3-1.4 wt.%, respectively.

3.3 Matrix

Table 3 and Fig. 6 show the average compositions of matrices in the three chondrites. These compositions overlap with those in CMs, COs, and Acfer 094. They plot along the serpentine line, which might indicate that serpentine is the major component of the matrices. However, the average totals of the matrices by EPMA are 90-96 wt.%. These totals are higher than those of phyllosilicates. Such high totals have previously been reported in the CM NWA 11024 that experienced secondary heating (Ebert et al., 2019). In contrast to NWA 11024 there is little evidence for heating of the three Asuka samples. The average apparent S weight percent in the matrices of the Asuka samples is 4-5 wt.%. Such high S contents are consistent with abundant sulfide grains of submicron size in the matrices.

3.4 X-ray diffraction

We measured the XRD patterns for the three Asuka CM chondrites. No phyllosilicates or tochilinite were detected in A 12169 and A 12236 (Fig. 7a), in spite of the fact that rare or minor phyllosilicates are present within their chondrules. Only A 12085 contains a small amount of cronstedtite (2θ=12.3°) and tochilinite (2θ=16.4°). From the high modal abundance of the matrix, we suggest that phyllosilicate and tochilinite are mainly present in the matrix of A 12085, although phyllosilicate does also occur in the chondrules of A 12085. These relationships suggest that the degree of alteration of A 12085 is somewhat higher than that of the other two chondrites. No

299 detection of phyllosilicate in A 12169 and A 12236 by the XRD indicates that their matrices are
300 mainly comprised of anhydrous minerals or amorphous phases. Since typical TCI is not observed
301 in A 12085, the occurrence of tochilinite is not yet evident. We need to undertake a further TEM
302 study to clarify this.

303 Olivine and clinoenstatite were identified by their XRD patterns (Figs. 7a and 7b). Figure 7b
304 shows that fayalitic olivine is encountered only in A 12169. The peak position, 31.9°, indicates
305 ~Fa_{50} olivine after the method by Imae and Nakamuta (2018). A small amount of orthoenstatite is
306 also seen in these chondrites. Kamacite, taenite, and troilite were commonly identified in the three
307 chondrites (Fig. 7c). Pyrrhotite was not detected by the XRD, although minor pyrrhotite is
308 identified by EPMA analysis. The major sulfide in these chondrites is troilite. Howard et al. (2009)
309 identified magnetite in CMs by the XRD technique. However, this phase was not identified in
310 these three chondrites, although rare magnetite was observed by FESEM as mentioned above.
311

312 3.5 Raman spectroscopy

313 The degree of heating experienced by the meteorites was evaluated using Raman
314 spectroscopy of matrix grains. For unequilibrated ordinaty chondrites (UOC), the full-width at
315 half-maximum (FWHM) of the D-band decreases with increasing heating temperature, and the
316 intensity ratio I_D/I_G increases (Quirico et al. 2003). This constraint has been successfully applied to
317 type 2 and type 3 carbonaceous chondrites (Bonal et al. 2006; Bonal et al., 2007; Quirico et al.
318 2014).

319 The matrix Raman spectra from the three chondrites in this study exhibit first-order carbon D-
320 and G-bands at ~1350 cm^{-1}, and ~1600 cm^{-1}, respectively. Average I_D/I_G ratios are 0.836, 0.848,
321 0.841, and 0.931, and FWHM-D are 351.6, 355.8, 343.8, and 269.1 cm^{-1}, for A 12085, A 12169, A

12236, and Murchison, respectively. These data are plotted in Fig. 8. All of the Asuka samples show broad FWHM-D and low I_D/I_G, and plot within the area of primitive CR chondrites (Komatsu et al., 2018). The matrix Raman characteristics of these three samples are distinguished from other CMs, including Murchison (subtype 2.5), heated CMs, and COs and CVs of higher petrologic types, indicating that they experienced very little heating.

We also measured some additional phases in these chondrites. Some mesostasis phases are plagioclase with distinct peaks at 505 cm^{-1}, and 487 cm^{-1}, and glass with a broad peak at ~500 cm^{-1}. We also identified calcite with a distinct peak at 1089 cm^{-1}.

3.6 Bulk compositions

Table 5 shows the bulk chemical composition of A 12236. Figure 9a shows Al/Mn versus (Zn/Mn)x100 ratios of the samples. A 12236 plots within the area of CMs. Figure 9b shows the CI-normalized bulk composition of A 12236, compared with those of Paris (CM2.7), Murchison (CM2.5), Nogoya (CM2.2), NWA 11024 (dehydrated CM), and CM-mean. A 12236 has a quite similar composition to those of other CMs, from refractory to volatile elements, except for a small depletion of Na and Pb. NWA 11024 experienced significant terrestrial weathering and is enriched in some elements, such as Li, K, and Pb. This enrichment is not apparent in A 12236 and other CMs. It is clear that A 12236 has bulk chemical composition typical of CMs.

3.7 Oxygen isotopes

The three Asuka CMs analyzed in this study have the following oxygen isotope compositions: A 12169: $\delta^{17}O$ -4.07 ‰; $\delta^{18}O$ 1.32 ‰; $\Delta^{17}O$ -4.75 ‰; A 12085: $\delta^{17}O$ -4.83 ‰; $\delta^{18}O$ -0.31 ‰; $\Delta^{17}O$ -4.67 ‰; A 12236: $\delta^{17}O$ -4.33 ‰; $\delta^{18}O$ 0.80 ‰; $\Delta^{17}O$ -4.75 ‰. These analyses are shown in Fig.

10 in relation to analyses of CM2, CO3 and anomalous C2 chondrites taken from the literature (full references to data sources are given in the caption to Fig. 10). The three Auska CMs plot away from the field of "normal" CM2 chondrites (Clayton and Mayeda, 1999; Haack et al., 2012; Hewins et al., 2014) and close to the field of CO3 falls (Alexander et al., 2018). The gap between the COs and CMs, where the Asuka CMs plot, is occupied by a range of C2 and anomalous CM chondrites (Greenwood et al., 2019; Lee et al., 2019). A number of these isotopically anomalous CM-like meteorites, such as LEW 85311 (Lee et al., 2019) and NWA 5958 show many mineralogical and petrological features typical of CMs, but like the Asuka CMs described here, have experienced only limited degrees of aqueous alteration. It therefore seems likely that the CM group extends from almost pristine examples that plot close to the CO3 field in Fig. 10, to highly aqueous altered examples that have isotopically heavy oxygen isotope compositions (top right corner of Fig. 10). EET 96029 (Lee et al., 2016) provides additional evidence in support of this relationship, containing areas which are both minimally altered (EET 96029 AK) and other areas which are heavily altered (EET 96029 OU). A linear regression line through the anomalous C2 samples in Fig. 10 ($y = -4.17 + 0.67x$ $R^2 = 0.95$) passes through the "normal" CM2 field. These relationships are consistent with the CM parent body having experienced highly variable levels of aqueous alteration. In addition, the fact that mildly altered samples, such as the Asuka CMs and NWA 5958, plot close to the CO3 field, and in the case of LEW 85311 actually plots within it, supports the original suggestion of Clayton and Mayeda (1999) that the anhydrous CM precursor material was CO-like, at least in terms of its oxygen isotope composition.

4. Discussion

4.1 Classification of chemical group

368 At first, we discuss the chemical group classification of these Asuka chondrites in comparison
369 with the other C chondrites. They have characteristic features as follows; 1) The modal
370 abundances of chondrule and matrix (Table 1) are similar to those in CMs (Weisberg et al., 2006).
371 The especially high abundance of matrix characterizes CM chondrites. 2) Chondrule size
372 distribution (Table 2) resembles that of CMs (Weisberg et al., 2006). 3) Refractory inclusions are
373 commonly encountered, and their abundances are within the range of CMs (Table 1). 4) Fe-Ni
374 metal is present, although it is more abundant than typical CMs (Table 1). 5) The Fe-Mn
375 distribution in olivines in the Asuka samples is also consistent with that of "normal" CMs (Fig. 3a),
376 although COs have a similar trend (Schrader and Davidson, 2017). 6) Porphyritic and type I
377 chondrules are highly abundant (Table 2), which is also the case for CMs (Jones, 2012). 7) The
378 bulk composition of A 12236 is close to those of other CMs (Fig. 9a and 9b).
379 These features distinguish these three chondrites from those of other major C chondrite
380 groups such as COs and CVs, and ungrouped C chondrites, such as Acfer 094 (Newton et al.,
381 1995) and Y-82094 (Kimura et al., 2014). A 12085, A 12169, and A 12236 are, therefore,
382 classified as belonging to the CM group. This classification is further supported by the abundances
383 and isotopic compositions of H, C, and N in A 12236 by Nittler et al. (2020).
384
385 4.2 Primitive natures and secondary processes
386 4.2.1 Aqueous alteration
387 Rubin et al. (2007) and Rubin (2015) suggested that CMs are classified into subtypes 2.7-2.0,
388 based on many petrologic criteria that reflect the alteration degree. Here we discuss the alteration
389 degree of the Asuka CMs studied here on the basis of the subtype criteria.

Chondrule mesostasis: The mesostases in chondrules of subtype 2.7-2.0 are replaced by phyllosilicates (Rubin, 2007). The chondrules in the Asuka CMs also contain phyllosilicates, with the abundances increasing from A 12169 through A 12236 to A 12085. In most chondrules of A 12169, phyllosilicate, if it present, replaces the primary mesostasis only in the peripheries. On the other hand, primary mesostasis phases (feldspar and glass) are abundant, not only in A 12169, but also in A 12236 and A 12085. All these results suggest low degrees of alteration, lower than in subtype 2.7.

Matrix phyllosilicates: CMs of subtypes 2.7-2.0 contain abundant phyllosilicates in their matrices. Phyllosilicates were identified only in the matrix of A 12085 by XRD. In A 12169 and A 12236, phyllosilicate were not detected in the matrices by XRD. Noguchi et al. (2020) observed no phyllosilicates in the matrix of A 12169 in TEM observations. These results indicate a lower degree of alteration for A 12169 and A 12236 than in those of subtypes 2.7-2.0.

Matrix compositions: The matrix compositions, MgO/FeO and S/SiO_2 weight ratios, can be used to classify the subtypes and increase and decrease with decreasing subtypes, respectively (Rubin et al., 2007). The MgO/FeO and S/SiO_2 ratios are 0.59 and 0.14, 0.51 and 0.12, and 0.56 and 0.16, in A 12169, A 12236, and A 12085, respectively. These values overlap with or are higher than those in subtypes 2.7-2.0 (0.35-0.7 for MgO/FeO and 0.05-0.18 for S/SiO_2).

Abundance of metal: The metal abundances in CMs decrease with decreasing subtype. The modal abundances of Fe-Ni metal in the Asuka CMs are 1.2-2.3 vol.%, which are similar to or higher than those in even subtype 2.7 (<2 vol.%). In particular, metal (2.3 vol.%) is much more abundant in A 12169 than any known CM.

Phenocrysts in chondrules: Alteration features in phenocryst are common in subtypes 2.3-2.0. On the other hand, all chondrules in the Asuka CMs have no any altered phenocrysts.

TCI: The abundance and occurrence of TCI and its composition are also criteria for the classification into subtypes. However, the Asuka CMs do not contain typical TCI. Tsuchiyama et al. (2020) reported possible precursors of TCI, Fe-rich hydrous silicate objects, in the matrix of A 12169 by TEM observation. Although fine-grained aggregates of sulfide and anhydrous silicates are observed, especially in A 12085, they are not TCI.

Sulfide: Pyrrhotite and pentlandite in CMs and CRs are proposed to be primary sulfide phases that originated under high-temperature conditions (Schrader et al., 2016; Singerling and Brearley, 2018). A 12169 contains such an assemblage (Fig. 2i), and they may represent high-temperature products. On the other hand, the abundances of pentlandite and pyrrhotite are also the criteria for the subtypes, and pentlandite increases with decreasing subtype (Rubin et al., 2007). The major sulfide is troilite in the Asuka CMs. On the other hand, troilite hardly remains in the other CMs, except in heated CMs (Nakamura, 2005).

Carbonate: Carbonate and its composition characterize the alteration degree. Ca-carbonate is encountered in subtypes 2.7-2.0. However, it is rarely encountered in these chondrites. Chondrules in A 12085 do contain some Ca-carbonate, whereas a tiny grain of Ca-carbonate occurs only in a clast in A 12169.

Thus, most of these criteria for subtypes 2.7-2.0 cannot be applied to the classification of A 12085, A 12169, and A 12236. Instead, many characteristic features of these chondrites indicate lower degrees of aqueous alteration for these chondrites, suggesting higher subtypes than 2.7. We will discuss the subtypes for the Asuka CMs in a later section. The common occurrence of unaltered melilite, especially in A 12169, provides additional support for these chondrites having experienced very limited degrees of aqueous alteration, because melilite is easily altered by secondary processes (Greenwood et al., 1994; Russell et al., 1998; Rubin, 1998). The degree of

alteration increases from A 12169, through A 12236, to A 12085. From the occurrence of phyllosilicate and carbonate, the degree of aqueous alteration is higher for A 12085 than A 12236 and lower than for a CM2.7 such as Paris and others which abundantly contains phyllosilicate and TCI (Hewins et al., 2014; Rubin 2007).

4.2.2 Secondary heating

Many CM or CM-related chondrites experienced heating (dehydration) after the aqueous alteration. Nakamura (2005) and Kimura et al. (2011) proposed the classification criteria for the degree of heating, such as decomposition of phyllosilicates and sulfide texture. A wide variety of silicate compositions indicate that these chondrites did not experience significant prolonged heating. From mineralogy, A 12085, A 12169, and A 12236 belong to stage I of Nakamura (2005), suggesting that they did not experience heating higher than 250 °C. This is supported by the occurrence of glass and clinoenstatite in chondrules, and the lack of ferroan rims on AOA olivines. Feldspar does not show devitrification texture with high-Ca pyroxene. Such an occurrence supports that proposition that little or no heating took place.

Rare plessitic features, a positive correlation between Ni and Co, and the compositional distribution of Si, P, and Cr in Fe-Ni metal are only observed in very primitive chondrites, such as Acfer 094 that did not experience secondary heating (Kimura et al., 2008 and 2011). The Asuka CMs have all these features in their Fe-Ni metal.

In heated CMs, pyrrhotite commonly has pentlandite blebs or lamella. On the other hand, such blebs and lamella in pyrrhotite are rare in uhheated CMs (Category A after Kimura et al., 2011). The Asuka CMs show similar features to unheated CMs (Kimura et al., 2011). Therefore, the Asuka CMs are classified as Category A.

459 The Raman spectral features of the matrices also indicate low degrees of heating. The Asuka
460 CMs plot within the range of unheated CR chondrites (Komatsu et al., 2018), and are distinct from
461 those of heated CMs, and metamorphosed CO, CV, and ordinary chondrites (Fig. 8). The matrices
462 of the Asuka CMs contain abundant S due to the presence of submicron sulfide grains. Abundant
463 and finely disseminated S in matrix is a feature of other primitive (almost unheated) chondrites
464 (e.g., Grossman and Brearley, 2005).

465 We conclude that the Asuka CMs did not experienced any heating. Therefore, we suggest that
466 the absence or rare occurrence of phyllosilicates and TCIs in the Asuka CMs are not the result of
467 thermal decomposition, but rather reflect the very limited aqueous alteration that these chondrites
468 have experienced.

469

470 4.2.3 Pristine CMs

471 Recently some CM or CM-related chondrites have been reported to have mineralogies
472 consistent with having experienced relatively low degrees of aqueous alteration, as mentioned
473 before. However, Paris, EET 96029, and LEW 85311 are classified as CM2.7, and still contain
474 abundant phyllosilicates (Hewins et al., 2014; Lee et al., 2016; Lee et al., 2019). CM-related NWA
475 5958 contains phyllosilicate and TCI. NWA 11024 is classified as type 3, but it experienced
476 secondary dehydration after weak aqueous alteration. All these chondrites seem to show higher
477 degrees of alteration than A 12169 and others. Therefore, these Asuka chondrites studied here,
478 especially A 12169, are the most primitive CM so far reported.

479 Noguchi et al. (2020) found predominant amorphous materials with enstatite whisker and no
480 phyllosilicate in the matrix of A 12169 in a TEM study. They suggested that the alteration degree
481 of A 12169 is lower than Paris. Nittler et al. (2020) suggested that A 12236 is the most pristine CM

482 from the isotopic compositions and abundance of H, C, and N, and abundant presolar grains. All
483 these results are consistent with our conclusions.
484
485 4.3 Classification of petrologic type
486 All CM chondrites were originally classified as petrologic type 2 (Van Schmus and Wood,
487 1967). Later many different criteria were proposed to classify varying degrees of alteration that
488 were experienced by the CMs, such as the matrix features (McSween, 1979), mineralogical index
489 (Browning et al., 1996), petrological features (Rubin et al., 2007), the analysis of H, C, and N
490 (Alexander et al., 2013), and phyllosilicate fraction (Howard et al., 2015). Among them, the
491 scheme of Rubin et al. (2007) is widely used as it provides a relatively straightforward means of
492 classifying the CMs and accordingly we use it here to assign the Asuka CMs to their appropriate
493 subtypes.
494 Rubin et al. (2007) and Rubin (2015) proposed subtypes for CMs that were not heated. Since
495 the Asuka CMs studied here are not only unheated, but also unbrecciated, they are suitable
496 samples for the application of the Rubin et al. (2007) and Rubin (2015) schemes. The Asuka CMs
497 should be assigned subtypes that are higher than 2.7 as discussed above. Rubin et al. (2007)
498 hypothesized that CM3.0 samples would have some distinct features that would help to identify
499 them, such as the occurrence of chondrule glass and minor phyllosilicate. Based on the results of
500 our study of the Asuka CMs, we have modified the scheme of Rubin et al. (2007) and propose the
501 following criteria for CM3.0 to 2.8 (Table 6).
502 CM3.0: The most distinguishing feature of this subtype is the abundant primary glass and
503 feldspar in chondrule mesostasis. Phenocrysts in chondrules do not show any alteration features.
504 Phyllosilicates are rarely encountered in chondrules. A small amount of phyllosilicate is also

observed in other primitive chondrites, such as ALH 77307 (CO3.03). However, no chondrules with completely altered mesostasis were observed. The matrix has no phyllosilicate, and the compositions, MgO/FeO and S/SiO_2 ratios are >0.5 and >0.1, respectively. TCI and carbonate are absent in them. Although the A 12169 section contain tiny Ca-carbonate, it is only in a clast. Fe-Ni metal is abundant, >2 vol.%, in chondrules and matrix. The major sulfide is troilite, although minor pyrrhotite-pentlandite is present. Harju et al. (2014) proposed the criteria for hypothetical "CR3", such as abundant glass in chondrules, no phenocryst alteration, and no phyllosilicate in the matrix. These criteria are nearly the same as those for CM3.0 presented here.

CM2.9: The primary mesostasis abundantly survives in chondrules. However, about half of the chondrules have partly to completely altered mesostasis. Phyllosilicates are not detected by the XRD because of their minor abundance. No occurrence of TCI and carbonate, and the abundance of troilite is nearly the same as subtype 3.0, although the metal abundance is 1-2 vol. %.

CM 2.8: In chondrules, phyllosilicate is more abundant than primary mesostasis, although phenocrysts are not yet altered. Only a minor amount of phyllosilicate is present, mainly in the matrix. Tochilinite is also detected by the XRD, although typical TCI is not observed. The metal abundance is nearly the same as CM2.9. Troilite is still the major sulfide mineral. Carbonate may be present.

From these criteria, A 12169, A 12236, and A 12085 are classified as subtype 3.0, 2.9, and 2.8, respectively. Although the three Asuka CMs have similar features such as petrography and oxygen isotopic compositions, the alteration degrees (subtypes) are evidently different and they were recovered from the wide area, as mentioned above. Therefore, it is an open question as whether these samples are paired and we cannot totally exclude the possibility that they represent different lithologies from the same breccia.

528

529 4.4 Primitive features of CM chondrites

530 Most CMs so far described experienced some combination of aqueous alteration, heating, and
531 brecciation, and have lost many of their primary features. On the other hand, the Asuka CMs, in
532 particular A 12169 CM3.0, hardly experienced these secondary processes. The terrestrial
533 weathering degrees also low. Therefore, these chondrites provide a unique opportunity to explore
534 the primary features of CM chondrites, as well as potential genetic relationships amongst the
535 CM-CO clan chondrites.

536 From the characteristic features of the Asuka CMs, we infer that unmodified chondrules and
537 refractory inclusions in CMs have many features that are common to all C chondrite groups, such
538 as abundant porphyritic chondrules with unaltered phenocrysts that are predominantly type I, pure
539 forsteritic olivine in AOAs, melilite-bearing CAIs, and the occurrence of Fe-Ni metal and troilite.
540 Primary matrix materials consisted of anhydrous minerals or amorphous phases. Amorphous
541 materials have also been reported in the matrices of some primitive CMs and COs (e.g., Brearley,
542 1993; Leroux et al. 2015; Davidson et al. 2019). Fayalitic olivine (~Fa_{50}) was only detected in A
543 12169 by XRD, although Noguchi et al. (2020) also reported similar olivine from the matrix of A
544 12169 in TEM study. Such ferroan olivine was also discovered in the matrices of other primitive C
545 chondrites (e.g., Brearley, 1993; Scott and Krot, 2006). All these primary features were partly to
546 completely lost from most CMs during aqueous alteration.

547 The CMs, including the Asuka CMs, have lower abundances of refractory inclusions and
548 opaque minerals but higher abundances of matrix when compared to all other types of C
549 chondrites. These features should be unique original features of CMs from the stage of precursor
550 materials. A 12236 (CM2.9), Paris (CM2.7), Murchison (2.5), and Nogoya (2.2) have quite similar

bulk compositions to each other, in spite of the wide variation in degree of aqueous alteration. This suggests that the bulk chemistry was not changed during aqueous alteration, as suggested by Rubin et al. (2007).

Kallemeyn and Wasson (1982) proposed that the CM and CO chondrites shared the same parent body and constituted a CM-CO clan. However, since CMs were aqueously altered unlike the COs, it has been difficult to compare the precursor materials to both groups. However, we can suggest that the primary materials of the CMs and COs were different from one another, especially chondrule size, the abundances of matrix, inclusions, and opaque minerals, and bulk compositions, as also suggested by Schrader and Davidson (2017) and Chaumard et al. (2018). Although the CMs and COs had anhydrous minerals with similar oxygen isotopic compositions (Kallemeyn and Wasson, 1982), COs contained the smaller chondrules and lower abundances of the matrix and refractory inclusions than primitive CMs. Therefore, we suggest that CMs and COs were derived from different parent bodies. Later, COs experienced very mild aqueous alteration and varying degrees of thermal metamorphism (e.g., Sears et al., 1991). On the other hand, most CMs were weakly to heavily subjected to aqueous alteration. Later some CMs experienced varying degrees of heating in their parent body. The results obtained here indicate that the CM parent body experienced very variable degrees of aqueous alteration.

While the CO and CM chondrites appear to show clear mineralogical and petrological differences, from an oxygen isotope perspective, both groups exhibit clear affinities (Fig. 10). The precursor material to the CMs, appears to have been isotopically nearly identical to that of the CO falls. It appears likely that both groups originated from a similar mix of primary components, with the likely distinction that CMs contained a higher content of volatile constituents (water ice?). This suggests that the parent bodies to both groups may have accreted in a similar region of the nebula.

574 It has been suggested by Chaumard et al. (2018) that chondrules in COs and CMs may have
575 formed in the same disk location, but that the CO parent body accreted before that of the CM. They
576 suggested that between these two accretion events the snow line may have moved inwards, such
577 that the CO parent body formed without a significant water ice fraction, whereas the CM parent
578 body did. Our study of the Asuka CMs, particularly their oxygen isotope compositions, further
579 highlights the strong relationship between CMs and COs, while also indicating that they are
580 probably not both derived from a single heterogeneous parent body.
581

582 **5. Conclusions**

583 We studied three Asuka carbonaceous chondrites. They are CMs, based on their modal
584 compositions, chondrule size distributions, and bulk compositions. They experienced minimal to
585 weak secondary processes such as aqueous alteration and heating. The degree of alteration
586 increases from A 12169, through A 12236, to A 12085, and we propose that they are classified as
587 subtypes 3.0 to 2.8, respectively.

588 We suggest that these chondrites, especially A 12169, are the most primitive CMs so far
589 described. These new CMs provide a unique opportunity to investigate the primary features of
590 CMs, as well as the genetic relationships of CM-CO clan chondrites. While showing strong
591 affinities in terms of their oxygen isotope compositions, CMs and COs were probably derived
592 from different parent bodies.

593 The CMs experienced complicated parent body processes. However, the classification
594 scheme proposed here is useful, not only for classification purposes, but the exploration of the
595 precursor materials and the history and evolution of the CM parent body.

The asteroids Ryugu and Bennu are related to hydrated chondrites, especially CMs (e.g., Hamilton et al., 2019; Morota et al., 2020), although Ryugu may have experienced heating by the Sun. On the other hand, the Asuka CMs studied here hardly experienced hydration and heating. However, as breccias are common in CM chondrites (Metzler et al., 1992) and the surface materials of the Ryugu and Bennu are highly variable, we expect that returned samples may contain some of the least altered materials, comparable to the Asuka CMs. Therefore, these chondrites are also of particular significance in view of the imminent return of sample material from the asteroids Ryugu and Bennu.

Acknowledgements

The sections were loaned from the National Institute of Polar Research. One of Murchison sections was loaned from T. Fagan. We appreciate the thoughtful reviews by two anonymous reviewers. We also thank the associate editor Kevin Righter for efficient handling of the manuscript. This work was supported by a Grant-in-aids of Ministry of Education, Science, Sport, and Culture of Japanese government, No. 18K03729 to M. K. This study was also supported by National Institute of Polar Research (NIPR) through Project research KP307 and General Collaboration Project no. 30-21. Oxygen isotope studies at the Open University are funded by a consolidated grant from the Science and Technology Facilities Council (STFC), UK GRANT NUMBER: ST/P000657/1.

References

618 Alexander, C.M.O.D., Howard, K.T., Bowden, R., Fogel, M.L., 2013. The classification of CM
619 and CR chondrites using bulk H, C and N abundances and isotopic compositions.
620 Geochimica et Cosmochimica Acta. 123, 244-260.
621 Alexander C. M. O'D., Greenwood R. C., Bowden R., Gibson J. M., Howard K. T. and Franchi I.
622 A. (2018) A multi-technique search for the most primitive CO chondrites. Geochim.
623 Cosmochim. Acta 221, 406-420.
624 Anders, E., Grevesse, N., 1989. Abundances of the elements: Meteoritic and solar. Geochimica et
625 Cosmochimica Acta. 53, 197-214.
626 Barrat, J.A., Zanda, B., Moynier, F., Bollinger, C., Liorzou, C., Bayon, G., 2012. Geochemistry of
627 CI chondrites: Major and trace elements, and Cu and Zn Isotopes. Geochimica et
628 Cosmochimica Acta. 83, 79-92.
629 Bonal L, Quirico E, Bourot-Denise M, Montagnac G., 2006. Determination of the petrologic type of CV3
630 chondrites by Raman spectroscopy of included organic matter. Geochimica et Cosmochimica Acta
631 70, 1849-1863.
632 Bonal L, Bourot-Denise M, Quirico E, Montagnac G, Lewin E., 2007. Organic matter and metamorphic
633 history of CO chondrites. Geochimica et Cosmochimica Acta 71, 1605-1623.Brearley, A.J., 1993.
634 Matrix and fine-grained rims in the unequilibrated CO3 chondrite, ALHA77307: Origins and
635 evidence for diverse, primitive nebular dust components. Geochimica et Cosmochimica Acta. 57,
636 1521-1550.
637 Braukmüller, N., Wombacher, F., Hezel, D.C., Escoube, R., Münker, C., 2018. The chemical composition
638 of carbonaceous chondrites: Implications for volatile element depletion, complementarity and
639 alteration. Geochimica et Cosmochimica Acta. 239, 17-48.

640 Browning, L.B., McSween, H.Y.J., Zolensky, M.E., 1996. Correlated alteration effects in CM
641 carbonaceous chondrites. Geochimica et Cosmochimica Acta. 60, 2621-2633.
642 Busemann, H., Alexander, C.M.O'D., Nittler, L., R., 2007. Characterization of insoluble organic matter in
643 primitive meteorites by microRaman spectroscopy. Meteortics & Planetary Sciences. 42,
644 1387-1416.
645 Chaumard, N., Defouilloy, C., Kita, N.T., 2018. Oxygen isotope systematics of chondrules in the
646 Murchison CM2 chondrite and implications for the CO-CM relationship. Geochimica et
647 Cosmochimica Acta. 228, 220-242.
648 Clayton, R.N., Mayeda, T.K., 1984. The oxygen isotope record in Murchison and other carbonaceous
649 chondrites. Earth and Planetary Science Letters. 67, 151-161.
650 Clayton R. N. and Mayeda T. K. (1999) Oxygen isotope studies of carbonaceous chondrites. Geochim.
651 Cosmochim. Acta 63, 2089–2104.
652 Davidson, J., Alexander, C.M.O.D., Stroud, R.M., Busemann, H., Nittler, L.R., 2019. Mineralogy and
653 petrology of Dominion Range 08006: A very primitive CO3 carbonaceous chondrite. Geochimica
654 et Cosmochimica Acta. 265, 259-278.
655 Ebert, S., Patzek, M., Lentfort, S., Bischoff, A., 2019. Accretion of differentiated achondritic and
656 aqueously altered chondritic materials in the early solar system—Significance of an igneous
657 fragment in the CM chondrite NWA 12651. Meteoritics & Planetary Science. 54,
658 2985-2995.
659 Greenwood, R.C., Lee, M.R., Hutchison, R., Barber, D.J., 1994. Formation and alteration of CAIs
660 in Cold Bokkeveld (CM2). Geochimica et Cosmochimica Acta. 58, 1913-1935.

661 Greenwood, R.C., Franchi, I.A., Gibson, J.M., Benedix, G.K., 2012. Oxygen isotope variation in
662 primitive achondrites: The influence of primordial, asteroidal and terrestrial processes.
663 Geochimica et Cosmochimica Acta. 94, 146-163.
664 Greenwood R. C., Burbine T. H., Miller M. F., and Franchi I. A. 2017 Melting and differentiation
665 of early-formed asteroids: The perspective from high precision oxygen isotope studies:
666 Chemie der Erde-Geochemistry 77, 1-43.
667 Greenwood, R.C., Howard, K.T., King, A.J., Lee, M.R., Burbine, T.H., Frranchi, I.A., Anand, M.,
668 Findlay, R., Gibson, J.M. A. 2019. Oxygen isotope evidence for multiple CM parent bodies:
669 What will we learn from the Hayabusa2 and OSIRIS-Rex sample return mission? (abstract).
670 Lunar and Planetary Science. 50, 2132.
671 Grossman, J.N., Brearley, A.J., 2005. The onset of metamorphism in ordinary and carbonaceous
672 chondrites. Meteoritics & Planetary Science. 40, 87-122.
673 Haack, H., Grau, T., Bischoff, A., Horstmann, M., Wasson, J., Sørensen, A., Laubenstein, M., Ott,
674 U., Palme, H., Gellissen, M., Greenwood, R., Pearson, V. K., Franchi, I. A., Gabelica, Z.,
675 Schmitt-Kopplin, P., 2012 Maribo—A new CM fall from Denmark. Meteoritics & Planetary
676 Science, 47, 30-50.
677 Hamilton, V.E., Simon, A.A., Christensen, P.R., Reuter, D.C., Clark, B.E., Barucci, M.A., Bowles,
678 N.E., Boynton, W.V., Brucato, J.R., Cloutis, E.A., Connolly, H.C., Donaldson Hanna, K.L.,
679 Emery, J.P., Enos, H.L., Fornasier, S., Haberle, C.W., Hanna, R.D., Howell, E.S., Kaplan,
680 H.H., Keller, L.P., Lantz, C., Li, J.Y., Lim, L.F., McCoy, T.J., Merlin, F., Nolan, M.C., Praet,
681 A., Rozitis, B., Sandford, S.A., Schrader, D.L., Thomas, C.A., Zou, X.D., Lauretta, D.S.,
682 Highsmith, D.E., Small, J., Vokrouhlický, D., Bowles, N.E., Brown, E., Donaldson Hanna,
683 K.L., Warren, T., Brunet, C., Chicoine, R.A., Desjardins, S., Gaudreau, D., Haltigin, T.,

Millington-Veloza, S., Rubi, A., Aponte, J., Gorius, N., Lunsford, A., Allen, B., Grindlay, J., Guevel, D., Hoak, D., Hong, J., Schrader, D.L., Bayron, J., Golubov, O., Sánchez, P., Stromberg, J., Hirabayashi, M., Hartzell, C.M., Oliver, S., Rascon, M., Harch, A., Joseph, J., Squyres, S., Richardson, D., Emery, J.P., McGraw, L., Ghent, R., Binzel, R.P., Asad, M.M.A., Johnson, C.L., Philpott, L., Susorney, H.C.M., Cloutis, E.A., Hanna, R.D., Connolly, H.C., Ciceri, F., Hildebrand, A.R., Ibrahim, E.M., Breitenfeld, L., Glotch, T., Rogers, A.D., Clark, B.E., Ferrone, S., Thomas, C.A., Campins, H., Fernandez, Y., Chang, W., Cheuvront, A., Trang, D., Tachibana, S., Yurimoto, H., Brucato, J.R., Poggiali, G., Pajola, M., Dotto, E., Mazzotta Epifani, E., Crombie, M.K., Lantz, C., Izawa, M.R.M., de Leon, J., Licandro, J., Garcia, J.L.R., Clemett, S., Thomas-Keprta, K., Van wal, S., Yoshikawa, M., Bellerose, J., Bhaskaran, S., Boyles, C., Chesley, S.R., Elder, C.M., Farnocchia, D., Harbison, A., Kennedy, B., Knight, A., Martinez-Vlasoff, N., Mastrodemos, N., McElrath, T., Owen, W., Park, R., Rush, B., Swanson, L., Takahashi, Y., Velez, D., Yetter, K., Thayer, C., Adam, C., Antreasian, P., Bauman, J., Bryan, C., Carcich, B., Corvin, M., Geeraert, J., Hoffman, J., Leonard, J.M., Lessac-Chenen, E., Levine, A., McAdams, J., McCarthy, L., Nelson, D., Page, B., Pelgrift, J., Sahr, E., Stakkestad, K., Stanbridge, D., Wibben, D., Williams, B., Williams, K., Wolff, P., Hayne, P., Kubitschek, D., Barucci, M.A., Deshapriya, J.D.P., Fornasier, S., Fulchignoni, M., Hasselmann, P., Merlin, F., Praet, A., Bierhaus, E.B., Billett, O., Boggs, A., Buck, B., Carlson-Kelly, S., Cerna, J., Chaffin, K., Church, E., Coltrin, M., Daly, J., Deguzman, A., Dubisher, R., Eckart, D., Ellis, D., Falkenstern, P., Fisher, A., Fisher, M.E., Fleming, P., Fortney, K., Francis, S., Freund, S., Gonzales, S., Haas, P., Hasten, A., Hauf, D., Hilbert, A., Howell, D., Jaen, F., Jayakody, N., Jenkins, M., Johnson, K., Lefevre, M., Ma, H., Mario, C., Martin, K., May, C., McGee, M.,

Miller, B., Miller, C., Miller, G., Mirfakhrai, A., Muhle, E., Norman, C., Olds, R., Parish, C., Ryle, M., Schmitzer, M., Sherman, P., Skeen, M., Susak, M., Sutter, B., Tran, Q., Welch, C., Witherspoon, R., Wood, J., Zareski, J., Arvizu-Jakubicki, M., Asphaug, E., Audi, E., Ballouz, R.L., Bandrowski, R., Becker, K.J., Becker, T.L., Bendall, S., Bennett, C.A., Bloomenthal, H., Blum, D., Boynton, W.V., Brodbeck, J., Burke, K.N., Chojnacki, M., Colpo, A., Contreras, J., Cutts, J., Drouet d'Aubigny, C.Y., Dean, D., DellaGiustina, D.N., Diallo, B., Drinnon, D., Drozd, K., Enos, H.L., Enos, R., Fellows, C., Ferro, T., Fisher, M.R., Fitzgibbon, G., Fitzgibbon, M., Forelli, J., Forrester, T., Galinsky, I., Garcia, R., Gardner, A., Golish, D.R., Habib, N., Hamara, D., Hammond, D., Hanley, K., Harshman, K., Hergenrother, C.W., Herzog, K., Hill, D., Hoekenga, C., Hooven, S., Howell, E.S., Huettner, E., Janakus, A., Jones, J., Kareta, T.R., Kidd, J., Kingsbury, K., Balram-Knutson, S.S., Koelbel, L., Kreiner, J., Lambert, D., Lauretta, D.S., Lewin, C., Lovelace, B., Loveridge, M., Lujan, M., Maleszewski, C.K., Malhotra, R., Marchese, K., McDonough, E., Mogk, N., Morrison, V., Morton, E., Munoz, R., Nelson, J., Nolan, M.C., Padilla, J., Pennington, R., Polit, A., Ramos, N., Reddy, V., Riehl, M., Rizk, B., Roper, H.L., the, O.-R.T., 2019. Evidence for widespread hydrated minerals on asteroid (101955) Bennu. 2019. Nature Astronomy. 3, 332-340.

Harju, E.R., Rubin, A.E., Ahn, I., Choi, B.-G., Ziegler, K., Wasson, J.T., 2014. Progressive aqueous alteration of CR carbonaceous chondrites. Geochimica et Cosmochimica Acta. 139, 267-292.

Hewins, R.H., Bourot-Denise, M., Zanda, B., Leroux, J., Barrat, J.A., Humayun, M., Göpel, C., Greenwood, R.C., Franchi, I.A., Pont, S., Lorand, J.P., Cournède, C., Gattacceca, J.,

729 Rochette, P., Kuga, M., Marrocchi, Y., Marty, B., 2014. The Paris meteorite, the least altered
730 CM chondrite so far. Geochimica et Cosmochimica Acta. 124, 190-222.
731 Howard, K.T., Benedix, G.K., Bland, P.A., Cressey, G., 2009. Modal mineralogy of CM2
732 chondrites by X-ray diffraction (PSD-XRD). Part 1: Total phyllosilicate abundance and the
733 degree of aqueous alteration. Geochimica et Cosmochimica Acta. 73, 4576-4589.
734 Howard, K.T., Alexander, C.M.O.D., Schrader, D.L., Dyl, K.A., 2015. Classification of hydrous
735 meteorites (CR, CM and C2 ungrouped) by phyllosilicate fraction: PSD-XRD modal
736 mineralogy and planetesimal environments. Geochimica et Cosmochimica Acta. 149,
737 206-222.
738 Ikeda, Y., 1983. Alteration of chondrules and matrices in the four Antarctic carbonaceous
739 chondrites ALH-77307(C3), Y-790123(C2), Y-75293(C2), and Y-74662(C2). Mem. Natl.
740 Inst. Polar Res. Spec. Issue 30, 93-108.
741 Imae N., Debaille V., Akada Y., Debouge W., Goderis S., Hublet G., Mikouchi T., Van Roosbroek
742 N., Yamaguchi A., Zekollari H., Claeys P., Kojima H., 2015. Report of the JARE-54 and
743 BELARE 2012-2013 joint expedition to collect meteorites on the Nansen Ice Field,
744 Antarctica. Antarctic Record 59, 38-72.
745 Imae, N., Kimura, M., Yamaguchi, A., Kojima, H., 2019. Primordial, thermal, and shock features
746 of ordinary chondrites: Emulating bulk X-ray diffraction using in-plane rotation of polished
747 thin sections. Meteoritics & Planetary Science. 54, 919-937.
748 Imae, N., Nakamuta, Y., 2018. A new mineralogical approach for CO3 chondrite characterization
749 by X-ray diffraction: Identification of primordial phases and thermal history. Meteoritics &
750 Planetary Science. 53, 232-248.

751 Jacquet E., Barrat J-A., Beck P., Caste F., Gattacceca J., Sonzogni C. and Gounelle M. (2016).
752 Northwest Africa 5958: A weakly altered CM-related ungrouped chondrite, not a CI3.
753 Meteorit. Planet. Sci. 51, 851–869.
754 Jones, R.H., 2012. Petrographic constraints on the diversity of chondrule reservoirs in the
755 protoplanetary disk. Meteoritics & Planetary Science. 47, 1176-1190.
756 Kallemeyn, G.W., Wasson, J.T., 1981. The compositional classification of chondrites-I. The
757 carbonaceous chondrite groups. Geochimica et Cosmochimica Acta. 45, 1217-1230.
758 Kallemeyn, G.W., Wasson, J.T., 1982. The compositional classification of chondrites:III.
759 Ungrouped carbonaceous chondrites. Geochimica et Cosmochimica Acta. 46, 2217-2228.
760 Kallemeyn, G.W., Rubin, A.E., Wasson, J.T., 1994. The compositional classification of
761 chondrites: VI. The CR carbonaceous chondrite group. Geochimica et Cosmochimica Acta.
762 58, 2873-2888.
763 Kimura, M., Barrat, J.A., Weisberg, M.K., Imae, N., Yamaguchi, A., Kojima, H., 2014. Petrology
764 and bulk chemistry of Yamato-82094, a new type of carbonaceous chondrite. Meteoritics &
765 Planetary Science. 49, 346-357.
766 Kimura, M., Grossman, J.N., Weisberg, M.K., 2008. Fe-Ni metal in primitive chondrites:
767 Indicators of classification and metamorphic conditions for ordinary and CO chondrites.
768 Meteoritics and Planetary Science. 43, 1161-1177.
769 Kimura, M., Grossman, J.N., Weisberg, M.K., 2011. Fe-Ni metal and sulfide minerals in CM
770 chondrites: An indicator for thermal history. Meteoritics & Planetary Science 46, 431-442.
771 Kimura, M., Ikeda, Y., 1995. Anhydrous alteration of Allende chondrules in the solar nebula II:
772 Alkali-Ca exchange reactions and formation of nepheline, sodalite and Ca-rich phases in
773 chondrules. Proc. NIPR Symp. Antarc. Meteorites. 8, 123-138.

774 Kimura, M., Imae, N., Yamaguchi, A., Greenwood, R. C., Komatsu, M., Noguchi, T. 2019.
775 Primitive CM-related chondrites: their characteristic features and classification (abstract).
776 82nd Annual Meeting of the Meteoritical Society. #6042
777 Kimura, M., Mikouchi, T., Suzuki, A., Miyahara, M., Ohtani, E., El Goresy, A., 2009. Kushiroite,
778 $CaAlAlSiO_6$: A new mineral of the pyroxene group from the ALH 85085 CH chondrite, and
779 its genetic significance in refractory inclusions. American Mineralogist. 94, 1479-1482.
780 Kimura, M., Yamaguchi, A., Miyahara, M., 2017. Shock-induced thermal history of an EH3
781 chondrite, Asuka 10164. Meteoritics & Planetary Science. 52, 24-35.
782 Komatsu, M., Fagan, T.J., Mikouchi, T., Petaev, M.I., Zolensky, M.E., 2015. LIME silicates in
783 amoeboid olivine aggregates in carbonaceous chondrites: Indicator of nebular and asteroidal
784 processes. Meteoritics & Planetary Science. 50, 1271-1294.
785 Komatsu, M. et al., 2018. First evidence for silica condensation within the solar protoplanetary
786 disk. Proceedings of the National Academy of Sciences. 115, 7497-7502.
787 Krot, A.N., Keil, K., Scott, E., R., D., Goodrich, C.A., Weisberg, M.K., 2014. Classification of
788 Meteorites and Their Genetic Reltionships. In: Davis, A.M. (Ed.), Treatise on Geochemistry
789 1, Meteorites, Comets, and Planets 2nd Edition. Elsevier, Amsterdam, pp. 1-63.
790 Lee, M.R., Lindgren, P., 2016. Aqueous alteration of chondrules from the Murchison CM
791 carbonaceous chondrite: Replacement, pore filling, and the genesis of polyhedral serpentine.
792 Meteoritics & Planetary Science. 51, 1003-1021.
793 Lee, M.R., Lindgren, P., King, A.J., Greenwood, R.C., Franchi, I.A., Sparkes, R., 2016. Elephant
794 Moraine 96029, a very mildly aqueously altered and heated CM carbonaceous chondrite:
795 Implications for the drivers of parent body processing. Geochimica et Cosmochimica Acta.
796 187, 237-259.

797 Lee, M. R., Cohen, B. E., King, A. J., Greenwood, R. C., 2019. The diversity of CM carbonaceous
798 chondrite parent bodies explored using Lewis Cliff 85311. Geochimica et Cosmochimica
799 Acta, 264, 224-244.
800 Leroux, H., Libourel, G., Lemelle, L., Guyot, F., 2003. Experimental study and TEM
801 characterization of dusty olivines in chondrites: Evidence for formation by in-situ reduction.
802 Meteoritics & Planetary Science. 38, 81-94.
803 Leroux, H., Cuvillier, P., Zanda, B., Hewins, R.H., 2015. GEMS-like material in the matrix of the
804 Paris meteorite and the early stages of alteration of CM chondrites. Geochimica et
805 Cosmochimica Acta. 170, 247-265.
806 Lodders K. and Fegley B. Jr. 1998. The planetary scientist's companion. New York: Oxford
807 University Press. 371 p.
808 Marrocchi, Y., Gounelle, M., Blanchard, I., Caste, F., Kearsley, A.T., 2014. The Paris CM
809 chondrite: Secondary minerals and asteroidal processing. Meteoritics & Planetary Science.
810 49, 1232-1249.
811 McSween, H.Y., Jr., 1979. Alteration in CM carbonaceous chondrites inferred from modal and
812 chemical variations in matrix. Geochimica et Cosmochimica Acta. 43, 1761-1770.
813 Metzler, K., Bischoff, A., Stöffler, D., 1992. Accretionary dust mantles in CM chondrites:
814 Evidence for solar nebula processes. Geochimica et Cosmochimica Acta. 56, 2873-2897.
815 Miller, M.F., Franchi, I.A., Sexton, A.S., Pillinger, C.T., 1999. High precision Δ17O isotope
816 measurements of oxygen from silicates and other oxides: Methods and applications. Rapid
817 Comm. Mass Spec. 13, 1211-1217.
818 Morota, T., Sugita, S., Cho, Y., Kanamaru, M., Tatsumi, E., Sakatani, N., Honda, R., Hirata, N.,
819 Kikuchi, H., Yamada, M., Yokota, Y., Kameda, S., Matsuoka, M., Sawada, H., Honda, C.,

820 Kouyama, T., Ogawa, K., Suzuki, H., Yoshioka, K., Hayakawa, M., Hirata, N., Hirabayashi,
821 M., Miyamoto, H., Michikami, T., Hiroi, T., Hemmi, R., Barnouin, O.S., Ernst, C.M.,
822 Kitazato, K., Nakamura, T., Riu, L., Senshu, H., Kobayashi, H., Sasaki, S., Komatsu, G.,
823 Tanabe, N., Fujii, Y., Irie, T., Suemitsu, M., Takaki, N., Sugimoto, C., Yumoto, K., Ishida,
824 M., Kato, H., Moroi, K., Domingue, D., Michel, P., Pilorget, C., Iwata, T., Abe, M., Ohtake,
825 M., Nakauchi, Y., Tsumura, K., Yabuta, H., Ishihara, Y., Noguchi, R., Matsumoto, K.,
826 Miura, A., Namiki, N., Tachibana, S., Arakawa, M., Ikeda, H., Wada, K., Mizuno, T., Hirose,
827 C., Hosoda, S., Mori, O., Shimada, T., Soldini, S., Tsukizaki, R., Yano, H., Ozaki, M.,
828 Takeuchi, H., Yamamoto, Y., Okada, T., Shimaki, Y., Shirai, K., Iijima, Y., Noda, H.,
829 Kikuchi, S., Yamaguchi, T., Ogawa, N., Ono, G., Mimasu, Y., Yoshikawa, K., Takahashi, T.,
830 Takei, Y., Fujii, A., Nakazawa, S., Terui, F., Tanaka, S., Yoshikawa, M., Saiki, T.,
831 Watanabe, S., Tsuda, Y., 2020. Sample collection from asteroid (162173) Ryugu by
832 Hayabusa 2: Implications for surface evolution. 2020. Science. 368, 654-659.
833 Nakamura, T., 2005. Post-hydration thermal metamorphism of carbonaceous chondrites. Journal
834 of Mineralogical and Petrological Sciences. 100, 260-272.
835 Newton, J., Bischoff, A., Arden, J.W., Franchi, I.A., Geiger, T., Greshake, A., Pillinger, C.T.,
836 1995. Acfer 094, a uniquely primitive carbonaceous chondrite from the Sahara. Meteoritics.
837 30, 47-56.
838 Nittler, L.R., Alexander, C. M. O'D., Foustoukos, D., Patzer, A., Verdier-Paoletti, M.J. 2020.
839 Asuka 12236, the most pristine cm chondrite to date (abstract). Lunar and Planetary Science.
840 51, 2276.

Noguchi, T., Yasutake, M., Tsuchiyama, A., Miyake, A., Kimura, M., Yamaguchi, A., Imae, N., Uesugi, K., Takeuchi, A. 2020. Matrix mineralogy of the least altered CM-related chondrite Asuka 12169 (abstract). Lunar and Planetary Science. 51, 1666.

Quirico E, Raynal P-I, Bourot-Denise M., 2003. Metamorphic grade of organic matter in six unequilibrated ordinary chondrites. Meteoritics & Planetary Science. 38, 795-881.

Quirico, E., Orthous-Daunay, F.-R., Beck, P., Bonal, L., Brunetto, R., Dartois, E., Pino, T., Montagnac, G., Rouzaud, J.-N., Engrand, C., Duprat, J., 2014. Origin of insoluble organic matter in type 1 and 2 chondrites: New clues, new questions. Geochimica et Cosmochimica Acta. 136, 80-99.

Rubin, A.E., 1998. Correlated petrologic and geochemical characteristics of CO3 chondrites. Meteoritics & Planetary Science. 33, 385-391.

Rubin, A.E., 2004. Aluminian low-Ca pyroxene in a Ca-Al-rich chondrule from the Semarkona meteorite. American Mineralogist. 89, 867-872.

Rubin, A.E., 2015. An American on Paris: Extent of aqueous alteration of a CM chondrite and the petrography of its refractory and amoeboid olivine inclusions. Meteoritics & Planetary Science. 50, 1595-1612.

Rubin, A.E., Trigo-Rodríguez, J.M., Huber, H., Wasson, J.T., 2007. Progressive aqueous alteration of CM carbonaceous chondrites. Geochimica et Cosmochimica Acta. 71, 2361-2382.

Russell, S.S., Huss, G.R., Fahey, A.J., Greenwood, R.C., Hutchison, R., Wasserburg, G.J., 1998. An isotopic and petrologic study of calcium-aluminum-rich inclusions from CO3 meteorites. Geochimica et Cosmochimica Acta. 62, 689-714.

Schrader, D.L., Davidson, J., McCoy, T.J., 2016. Widespread evidence for high-temperature formation of pentlandite in chondrites. Geochimica et Cosmochimica Acta. 189, 359-376.

Schrader, D.L., Davidson, J., 2017. CM and CO chondrites: A common parent body or asteroidal neighbors? Insights from chondrule silicates. Geochimica et Cosmochimica Acta. 214, 157-171.

Scott, E.R.D., Krot, A.N., 2006. Thermal processing of silicate dust in the solar nebula: Clues from primitive chondrite matrices. Astrophysical Journal. 623, 571-578.

Sears, D.W.G., Batchelor, J.D., Lu, J., Keck, B.D., 1991. Metamorphism of CO and CO-like chondrites and comparisons with type 3 ordinary chondrites. Proc. NIPR Symp. Antarct. Meteorites. 4, 319-343.

Singerling, S.A., Brearley, A.J., 2018. Primary iron sulfides in CM and CR carbonaceous chondrites: Insights into nebular processes. Meteoritics & Planetary Science. 53, 2078-2106.

Starkey, N.A., Jackson, C.R.M., Greenwood, R.C., Parman, S., Franchi, I.A., Jackson, M., Fitton, J.G., Stuart, F.M., Kurz, M., and Larsen, L.M., 2016. Triple oxygen isotopic composition of the high 3He/4He mantle. Geochimica et Cosmochimica Acta 176, 227-238.

Stelzner, T., Heide, K., Bischoff, A., Weber, D., Scherer, P., Schultz, L., Happel, M., Schrön, W., Neupert, U., Michel, R., Clayton, R.N., Mayeda, T.K., Bonani, G., Haidas, I., Ivy-Ochs, S., Suter, M., 1999. An interdisciplinary study of weathering effects in ordinary chondrites from the Acfer region, Algeria. Meteoritics & Planetary Science. 34, 787-794.

Tenner, T.J., Nakashima, D., Ushikubo, T., Tomioka, N., Kimura, M., Weisberg, M.K., Kita, N.T., 2019. Extended chondrule formation intervals in distinct physicochemical environments: Evidence from Al-Mg isotope systematics of CR chondrite chondrules with unaltered plagioclase. Geochimica et Cosmochimica Acta. 260, 133-160.

886 Tsuchiyama, A., Noguchi, T., Yasutake, M., Miyake, A., Kimura, M., Yamaguchi, A., Imae, N.,
887 Uesugi, K., Takeuchi, A. 2020. Three-dimensional nano/microtexture of a least altered
888 CM-related chondrite Asuka 12169 (abstract). Lunar and Planetary Science. 51, 1801.
889 Van Schmus, W.R., Wood, J.A., 1967. A chemical-petrologic classification for the chondrite
890 meteorites. Geochimica et Cosmochimica Acta. 31, 747-765.
891 Wasson, J.T., Rubin, A.E., 2010. Matrix and whole-rock fractionations in the Acfer 094 type 3.0
892 ungrouped carbonaceous chondrite. Meteoritics & Planetary Science. 45, 73-90.
893 Weisberg, M.K., McCoy, T.J., Krot, A.N., 2006. Systematics and evaluation of meteorite
894 classification. in: Lauretta, D.S., McSween, H.Y., Jr. (Eds.), Meteorites and the Early Solar
895 System II. The University of Arizona Press, Tucson, pp. 19-52.
896 Wolf, D., Palme, H., 2001. The solar system abundances of phosphorus and titanium and the
897 nebular volatility of phosphorus. Meteoritics & Planetary Science. 36, 559-571.
898 Yamaguchi, A., Barrat, J.-A., Ito, M., Bohn, M., 2011. Posteucritic magmatism on Vesta:
899 Evidence from the petrology and thermal history of diogenites. Journal of Geophysical
900 Research. 116, E08009, 15 PP., 2011, https://doi:10.1029/2010JE003753.
901 Yamaguchi, A., Kimura, M., Pittarello, L., Imae, N., Debaille, V., Philippe, C., Kojima, H. 2016.
902 Meteorite Newsletter. 25.
903 Zolensky, M., Barrett, R., Browning, L., 1993. Mineralogy and composition of matrix and
904 chondrule rims in carbonaceous chondrites. Geochimica et Cosmochimica Acta. 57,
905 3123-3148.
906 Zolensky, M.E., Weisberg, M.K., Buchanan, P.C., Mittlefehldt, D.W., 1996. Mineralogy of
907 carbonaceous chondrite clast in HED achondrites and the Moon. Meteoritics & Planetary
908 Science. 31, 518-537.

909

910

911 **Figure captions**

912 Fig. 1. Backscattered electron (BSE) images of a) A 12085, 41-1 (width of sample 12.8 mm),
913 showing chondrules among matrix), b) A 12169, 31-1 (6.7 mm), containing fusion crusts in
914 both sides of the section (gray areas), and c) combined elemental (Mg-Ca-Al) map of A
915 12169 showing CAIs, and d) BSE image of A 12236, 51-1 (12.6 mm).

916 Fig. 2. BSE images of constituent components. a) A melilite (Mel) -rich CAI with spinel (Sp) and
917 high-Ca pyroxene (Hpx) in A 12169. The width is 210 µm. b) An AOA, consisting of
918 forsteritic olivine (Ol) with interstitial anorthite and high-Ca pyroxene (An+Hpx) and
919 kamacite (Kam) in A 12236. The width is 280 µm. c) A Type I chondrule in A 12169,
920 mainly consisting of phenocrysts of olivine and low-Ca pyroxene (Lpx), among feldspathic
921 mesostasis (light gray). The width is 0.76 mm. d) A Type I chondrule in A 12169
922 consisting of olivine, low- and high-Ca pyroxene, and glassy mesostasis (Gla). The width
923 is 240 µm. e) A type II chondrule in A 12085, consisting of ferroan olivine with abundant
924 relict forsteritic olivine (dark), surrounded by fine-grained rim. The width is 0.65 mm. f) A
925 peripheral part of type I chondrule in A 12085. Mesostasis is replaced by phyllosilicate
926 (Phy). The width is 170 µm. g) Homogeneous kamacite spherules in a type I chondrule of
927 A 12236. The width is 210 µm. h) A matrix area of A 12169, consisting of very
928 fine-grained silicate phases with abundant sulfide of submicron in size (bright). The width
929 is 20 µm. i) A sulfide grain in A 12169, consisting of pyrrhotite (Po) with small amounts of
930 pentlandite (Pn). The width is 190 µm. j) A type I chondrule and matrix area of A 12085,
931 including fine-grained aggregates of Fe-sulfide with silicate phases (Sul+Sil). The width is
932 210 µm.

933 Fig. 3. Olivine compositions. a) Fe vs. Mn plot of olivine from the Asuka chondrites, in
934 comparison with that of Murchison (CM2.5). b) Mean Cr_2O_3 vs. σ-Cr_2O_3 plot in ferroan
935 olivine for Asuka chondrites. The diagram and CO trend are after Grossman and Brearley
936 (2005) and Schrader and Davidson (2017). A dotted circle shows the area of CO3.0 and
937 CM chondrites.
938 Fig. 4. The mesostasis composition on (Si+Al)-Mg-Fe diagram (atomic ratio) for the Asuka
939 chondrites and other CM and CO chondrites.
940 Fig. 5. Ni vs. Co (wt.%) plot of Fe-Ni metal grains in the Asuka chondrites. The dotted line shows
941 the CI chondritic Co/Ni ratio after Anders and Grevesse (1989).
942 Fig. 6. Matrix compositions of the Asuka chondrites in atomic (Si+Al)-Mg-Fe plot, compared with
943 other CMs, COs, and Acfer 094 (this work; Metzler et al., 1992; Zolensky et al., 1993;
944 Marrocchi et al., 2014; Wasson and Rubin, 2010).
945 Fig. 7. a) X-ray diffraction of 2 theta, 0-30° for the Asuka chondrites, in comparison with A 12248
946 (CM2.0). b) Diffraction of 2 theta, 29-33.5°. c) Diffraction of 2 theta, 42.8-45.2°.
947 Ant=antigolite, Cro=cronstedtite, Cen=clinoenstatite, Fa=fayalitic olivine, Kam=kamacite,
948 Oen=orthoenstatite, Tae=taenite, Toc=tochilinite, and Tr=troilite.
949 Fig. 8. Spectral parameters of Raman bands of carbonaceous matter from the matrix of the Asuka
950 chondrites and Murchison. Dotted areas summarize data from the other chondrites. CRs,
951 COs, CVs, and UOCs are after Komatsu et al. (2018). CMs-B is after Buseman et al.
952 (2007), and CRs&CMs-Q is after Quirico et al. (2014).
953 Fig. 9. a) Al/Mn versus (Zn/Mn)x100 atomic ratios of the Asuka chondrites. Dotted areas for
954 chondrites are after Krot et al. (2014). b) The CI-normalized bulk composition of A 12236
955 (CM2.9), compared with those of Paris (CM2.7), Murchison (CM2.5), Nogoya (CM2.2),

NWA 11024 (dehydrated CM), and CM-mean. The data of Paris and Nogoya are after Hewins et al. (2014), Murchison after Wolf and Palme (2001) and Hewins et al. (2014), NWA 11024 after Ebert et al. (2019), and CM-mean after Lodders and Fegley (1998). In NWA 11024, the data of Sr, Ba, and U, are not plotted because of terrestrial weathering effect (Stelzner et al., 1999). The condensation temperatures for elements are after Lodders and Fegley (1998).

Fig. 10. Oxygen three isotope diagram showing the relationship between the Asuka CMs, anomalous C2 chondrites, “normal” CM2 chondrites and CO3 chondrites. The regression line shown was calculated using only the analyses of anomalous C2 samples. TFL = Terrestrial Fractionation Line. CCAM = Carbonaceous Chondrite Anhydrous Mineral line (Clayton and Mayeda, 1999). Data sources – “normal” CM2s: Clayton and Mayeda, 1999); Haack et al., 2012; Hewins et al., 2014, CO3 chondrite falls: Alexander et al. (2018); Anomalous C2 chondrites Clayton and Mayeda, 1999; with the exception of: EET 85311 “OU” and EET 85311 “AK” (Lee et al., 2016); LEW 85311 “Lee” (Lee et al., 2019); NWA 5958 (Jacquet et al., 2016).

Table 1. Modal abundance (vol. %) of components in A 12085, A 12169, and A 12236, compared with other CMs.

Sample	Subtype	Chondrule	Refractory inclusion	Matrix	Metal	Sulfide	*References*
A 12085	2.8	36.0	4.2	57.7	1.2	0.9	*This work*
A 12169	3.0	38.6	4.3	53.4	2.3	1.4	*This work*
A 12236	2.9	28.9	3.8	64.8	1.5	1.1	*This work*
Paris	2.7	<45	<1	55	1.2	0.7	*Hewins et al. (2014); Rubin (2015)*
EET 96029	2.7	17	1.8	78	0.3	1.2	*Lee et al. (2016)*
NWA 11024	"3.0"	32	1.2	64	2.4	0.5	*Ebert et al. (2019)*
CM		20	5	70	0.1		*Weisberg et al. (2016)*

Table 2. Characteristic features of chondrules in A 12085, A 12169, and A 12236, compared with other CMs.

Sample	Average diameter	Porphyritic chondrules	Type I chondrule[1)]	Atleration (%)[2)]			References
	(mm)	(%)	(%)	completely	partially	unaltered	
A 12085	0.31	97.5	90.3	22	56	22	*This work*
A 12169	0.26	95.2	92.2	0	36	64	*This work*
A 12236	0.29	97.9	91.8	2	50	48	*This work*
Paris	0.25						*Hewins et al. (2014); Rubin (2015)*
EET 96029	0.4						*Lee et al. (2016)*
NWA 11024	0.15-0.3						*Ebert et al. (2019)*
CM	0.3	95	90-90				*Weisberg et al. (2006); Jones (2012)*

[1)] Percentage of Type I in all chondrules.

[2)] See alteration degree in the text.

Table 3. Representative compositions of silicate and oxide phases and the average matrix composition.

Phase	Sample	Occurrence	Type	SiO_2	TiO_2	Al_2O_3	Cr_2O_3	V_2O_3	FeO	NiO	MnO	MgO	CaO	ZnO	Na_2O	K_2O	P_2O_5	SO_3	Total	Wo	En	Fs	An	Ab	Or
Feldspar	A 12169	Chondrule	I	46.44	b.d.	33.53	b.d.	b.d.	0.30	b.d.	0.10	0.77	19.61	b.d.	0.05	b.d.	b.d.	b.d.	100.81				99.4	0.4	0.2
Feldspar	A 12236	Chondrule	II	64.02	0.05	23.08	b.d.	b.d.	1.02	b.d.	b.d.	0.13	4.45	b.d.	8.66	0.30	b.d.	b.d.	101.71				21.7	76.6	1.7
Feldspar	A 12236	AOA		42.94	0.17	36.14	b.d.	b.d.	0.37	b.d.	b.d.	0.72	20.18	b.d.	b.d.	b.d.	b.d.	b.d.	100.51				99.8	0.2	0.0
Glass	A 12169	Chondrule	I	51.60	0.06	24.40	0.24	b.d.	1.25	b.d.	b.d.	8.42	13.75	b.d.	1.55	0.10	b.d.	b.d.	101.36				82.5	16.9	0.7
Melilite	A 12085	CAI		22.38	0.15	35.55	b.d.	b.d.	0.11	b.d.	b.d.	0.54	40.91	b.d.	b.d.	b.d.	b.d.	b.d.	99.63						
Olivine	A 12085	Chondrule	I	42.51	0.09	0.16	0.18	b.d.	0.11	b.d.	b.d.	56.78	0.42	b.d.	b.d.	b.d.	b.d.	b.d.	100.24						
Olivine	A 12085	Chondrule	II	37.05	b.d.	b.d.	0.30	b.d.	31.90	b.d.	0.26	30.85	0.32	b.d.	b.d.	b.d.	b.d.	b.d.	100.67						
Olivine	A 12085	AOA		42.87	0.09	b.d.	0.29	b.d.	0.26	b.d.	0.36	56.48	0.05	b.d.	b.d.	b.d.	b.d.	b.d.	100.40						
Phyllosilicate	A 12085	Chondrule	I	39.55	0.05	1.92	0.35	b.d.	20.92	0.26	0.65	14.85	1.60	b.d.	0.34	0.18	b.d.	1.07	81.72						
Phyllosilicate	A 12236	Chondrule	I	31.15	b.d.	12.68	b.d.	b.d.	31.88	b.d.	0.14	8.36	0.16	b.d.	0.29	0.27	0.17	0.36	85.45						
Merrilite	A 12085	Chondrule	II	0.62	0.08	0.47	b.d.	b.d.	2.21	b.d.	0.10	2.97	45.05	b.d.	2.67	b.d.	44.32	0.46	98.94						
High-Ca pyroxene	A 12085	Chondrule	I	52.45	0.51	4.28	1.01	b.d.	2.22	b.d.	0.36	25.01	13.02	b.d.	b.d.	b.d.	b.d.	b.d.	98.85	26.3	70.2	3.5			
High-Ca pyroxene	A 12236	Chondrule	II	51.03	0.16	0.62	1.03	b.d.	17.14	b.d.	0.36	11.01	16.89	b.d.	0.43	b.d.	b.d.	b.d.	98.66	37.1	33.6	29.4			
Kushiroite	A 12169	CAI		31.30	0.13	37.95	b.d.	b.d.	2.30	b.d.	b.d.	3.34	26.32	b.d.	b.d.	b.d.	b.d.	b.d.	101.33						
Low-Ca pyroxene	A 12169	Chondrule	I	58.80	0.28	0.99	0.40	b.d.	0.52	b.d.	0.08	37.53	0.54	b.d.	b.d.	b.d.	b.d.	b.d.	99.13	1.0	98.2	0.8			
Low-Ca pyroxene	A 12169	Chondrule	II	49.92	b.d.	0.13	0.43	b.d.	34.78	b.d.	0.28	12.48	0.40	b.d.	b.d.	b.d.	b.d.	b.d.	98.41	0.9	38.7	60.5			
Chromite	A 12085	Chondrule	II	0.25	0.96	9.24	54.56	0.64	26.96	b.d.	0.38	6.38	0.02	0.11	b.d.	b.d.	b.d.	b.d.	99.49						
Spinel	A 12169	AOA		b.d.	0.19	72.13	b.d.	0.18	0.25	b.d.	b.d.	27.54	0.20	b.d.	b.d.	b.d.	b.d.	b.d.	100.50						
Matrix	A 12085	Matrix		29.04	0.06	2.65	0.37	b.d.	28.46	1.80	0.23	15.90	0.68	b.d.	0.23	0.11	0.12	11.44	91.10						
Matrix	A 12169	Matrix		31.29	0.07	2.60	0.38	b.d.	29.63	1.74	0.24	17.48	0.81	b.d.	0.49	0.15	0.22	10.71	95.80						
Matrix	A 12236	Matrix		29.35	0.07	2.57	0.35	b.d.	30.03	1.76	0.24	15.43	0.59	b.d.	0.21	0.12	0.19	9.06	89.97						

b.d.: below detection limits (3 sigma), 0.03 for SiO_2, Al_2O_3, MgO, CaO, and SO_3, 0.04 for TiO_2, V_2O_3, Na_2O, K_2O, and P_2O_5, 0.08 for NiO and MnO, and 0.10 for Cr_2O_3 and ZnO.
* Matrix data was averaged composition.

Table 4. Representative compositions of opaque minerals.

Phase	Sample	Occurrence	Si	P	S	Cr	Fe	Co	Ni	Cu	Total
Kamacite	A 12085	Isolated	b.d.	0.18	b.d.	b.d.	93.25	0.29	5.42	0.07	99.21
Kamacite	A 12085	Chondrule	0.58	0.39	b.d.	0.99	92.81	0.28	4.88	b.d.	99.92
Kamacite	A 12236	Chondrule	b.d.	0.33	b.d.	0.33	92.33	0.33	5.50	0.08	98.89
Kamacite	A 12236	Chondrule	b.d.	0.35	b.d.	0.20	93.31	0.33	5.60	0.00	99.79
Ni-rich metal	A 12085	Chondrule	b.d.	b.d.	b.d.	b.d.	67.26	2.14	29.83	b.d.	99.23
Ni-rich metal	A 12169	Isolated	b.d.	b.d.	b.d.	b.d.	55.76	2.02	40.27	0.06	98.11
Ni-rich metal	A 12236	Isolated	b.d.	b.d.	b.d.	0.06	66.09	2.11	30.86	b.d.	99.12
Pentlandite	A 12169	Isolated	b.d.	b.d.	32.77	b.d.	34.41	0.93	30.62	0.20	98.93
Pentlandite	A 12236	Chondrule	b.d.	b.d.	32.73	b.d.	38.63	0.89	25.78	0.07	98.10
Pyrrhotite	A 12169	Isolated	b.d.	b.d.	36.87	b.d.	60.53	0.14	0.68	b.d.	98.21
Pyrrhotite	A 12236	Isolated	b.d.	b.d.	36.95	b.d.	58.76	0.33	2.28	b.d.	98.32
Troilite	A 12169	Isolated	b.d.	b.d.	35.69	b.d.	61.68	0.07	0.40	b.d.	97.84
Troilite	A 12236	Isolated	b.d.	b.d.	36.32	b.d.	62.10	0.08	0.24	b.d.	98.74

b.d.: below detection limits (3 sigma), 0.03 for Si and P, and 0.05 for S, Co, Ni, Cr, Fe, and Cu.

Table 5. Major and trace element abundances for A 12236.

ICP-AES		
TiO_2	wt%	0.11
Al_2O_3	wt%	2.17
FeO	wt%	30.25
MnO	wt%	0.23
MgO	wt%	19.95
CaO	wt%	1.77
Na_2O	wt%	0.37
K_2O	wt%	0.04
P_2O_5	wt%	0.23
Ni	wt%	1.36
Cr	µg/g	3177

ICP-MS		
Li	µg/g	1.72
Be	µg/g	0.0286
CaO	wt%	1.75
P_2O_5	wt%	0.24
K	µg/g	383
Sc	µg/g	8.88
TiO_2	wt%	0.0987
V	µg/g	66.78
Mn	µg/g	1597
Co	µg/g	558
Cu	µg/g	111
Zn	µg/g	162
Ga	µg/g	7.46
Rb	µg/g	1.90
Sr	µg/g	9.89
Y	µg/g	2.27
Zr	µg/g	5.15
Nb	µg/g	0.381
Cs	µg/g	0.103
Ba	µg/g	3.22

ICP-MS		
La	µg/g	0.325
Ce	µg/g	0.830
Pr	µg/g	0.126
Nd	µg/g	0.636
Sm	µg/g	0.208
Eu	µg/g	0.0785
Gd	µg/g	0.286
Tb	µg/g	0.0537
Dy	µg/g	0.364
Ho	µg/g	0.0809
Er	µg/g	0.238
Tm	µg/g	0.0358
Yb	µg/g	0.227
Lu	µg/g	0.0352
Hf	µg/g	0.153
Ta	µg/g	0.0187
W	µg/g	0.14
Pb	µg/g	1.26
Th	µg/g	0.0398
U	µg/g	0.00957

Table 6. Petrologic subtypes of CM chondrites, modified after Rubin (2015).

Petrologic subtype	3.0	2.9	2.8	2.7	2.6	2.5	2.4	2.3	2.2	2.1	2.0
Chondrule mesostases	Primary meso Rare Phyllo	Primary meso □ Phyllo	Phyllo>Primary meso	Phyllosilicate	Phyllosilicate	Phyllosilicate	Phyllosilicate	Phyllosilicate	Phyllosilicate	Phyllosilicate	Phyllosilicate
Matrix phyllosilicates	Rare or no	Rare	Minor	Abundant	Abundant	Abundant	Abundant	Abundant	Abundant	Abundant	Abundant
Matrix composition: MgO/"feo"	>0.5	>0.5	>0.5	0.35-0.43	0.35-0.43	0.35-0.43	0.35-0.43	0.50-0.70	0.50-0.70	0.50-0.70	0.50-0.70
Matrix composition: S/SiO_2	>0.1	>0.1	>0.1	0.10-0.18	0.10-0.18	0.10-0.16	0.10-0.16	0.07-0.08	0.07-0.08	0.05-0.07	0.05-0.07
Metallic Fe-Ni (vol%)	>2	1-2	1-2	1-2	~1	0.03-0.30	0.03-0.30	0.03-0.30	0.03-0.30	≤0.02	≤0.02
Phenocrysts in chondrules	Unaltered	Unaltered	Unaltered	Unaltered	Unaltered	Unaltered	Unaltered	2-15% altered	15-85% altered	85-99% altered	Completely altered
Large TCI clumps (vol%)	No TCI	No TCI	Minor	5-20	15-40	15-40	15-40	15-40	15-40	2-5	2-5
TCI composition: "FeO"/SiO_2				4.0-7.0	2.0-3.3	2.0-3.3	1.5-2.0	1.5-2.0	1.0-1.7	1.0-1.7	1.0-1.7
TCI composition: S/SiO_2				0.40-0.60	0.18-0.35	0.18-0.35	0.14-0.20	0.14-0.20	0.05-0.09	0.05-0.09	0.05-0.09
Sulfide	Tro > po + pn	Tro > po + pn	Tro > po + pn	po + pn	Mainly Po + pn	Mainly Po + pn	po + pn + int	po + pn + int	Mainly pn + int	Mainly pn + int	Mainly pn + int
Carbonate	No or rare carbonate	No or rare carbonate	Minor	Ca carbonate	Ca carbonate	Ca carbonate	Ca carbonate	Ca carbonate	Ca carbonate	Ca carbonate + complex carbonate	Ca carbonate + complex carbonate

Primary meso: primary feldspar and glass, tro: troilite, po: pyrrhotite, pn: pentlandite, int: sulfide grains with ''intermediate'' Ni/(Fe + Ni) ratios
Subtypes 2.7-2.0 are after Rubin (2015).

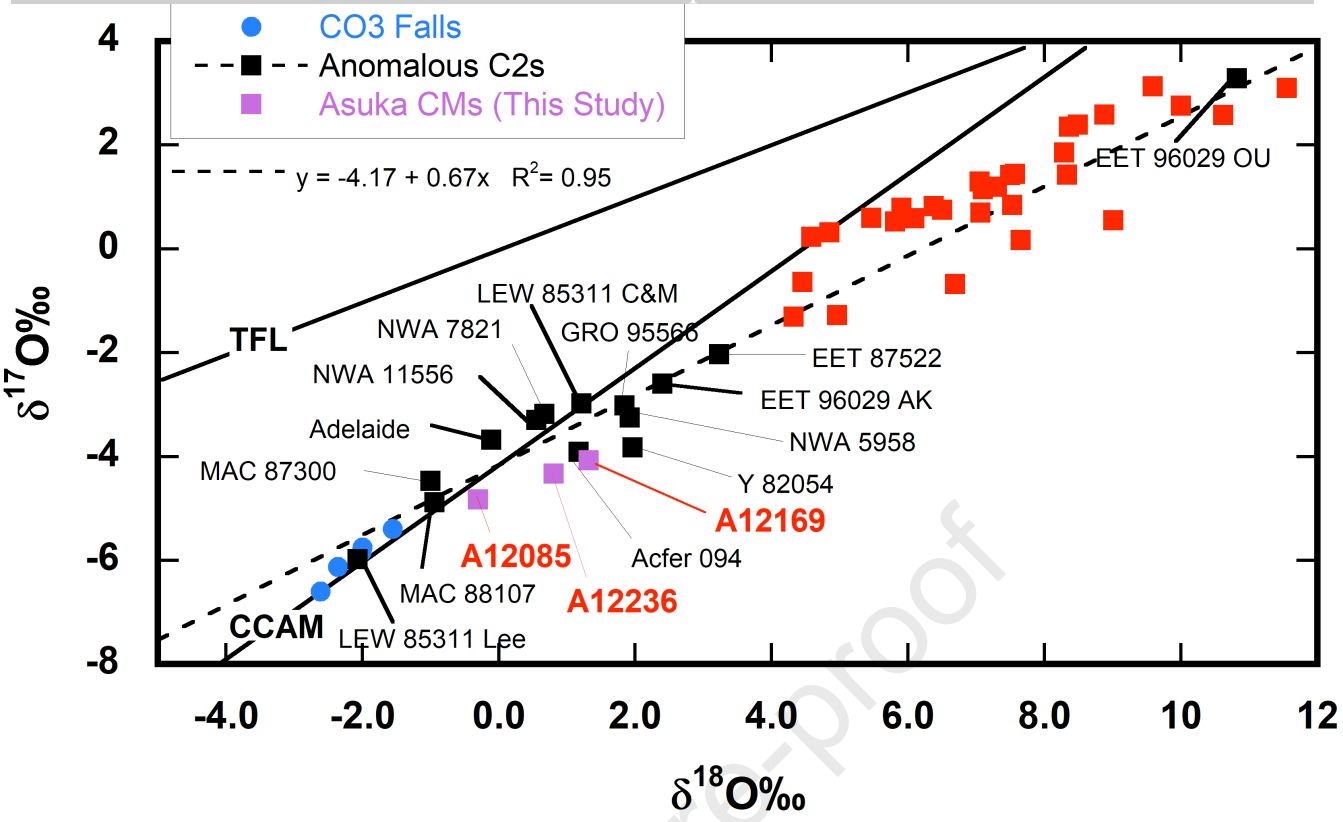

Fig. 10

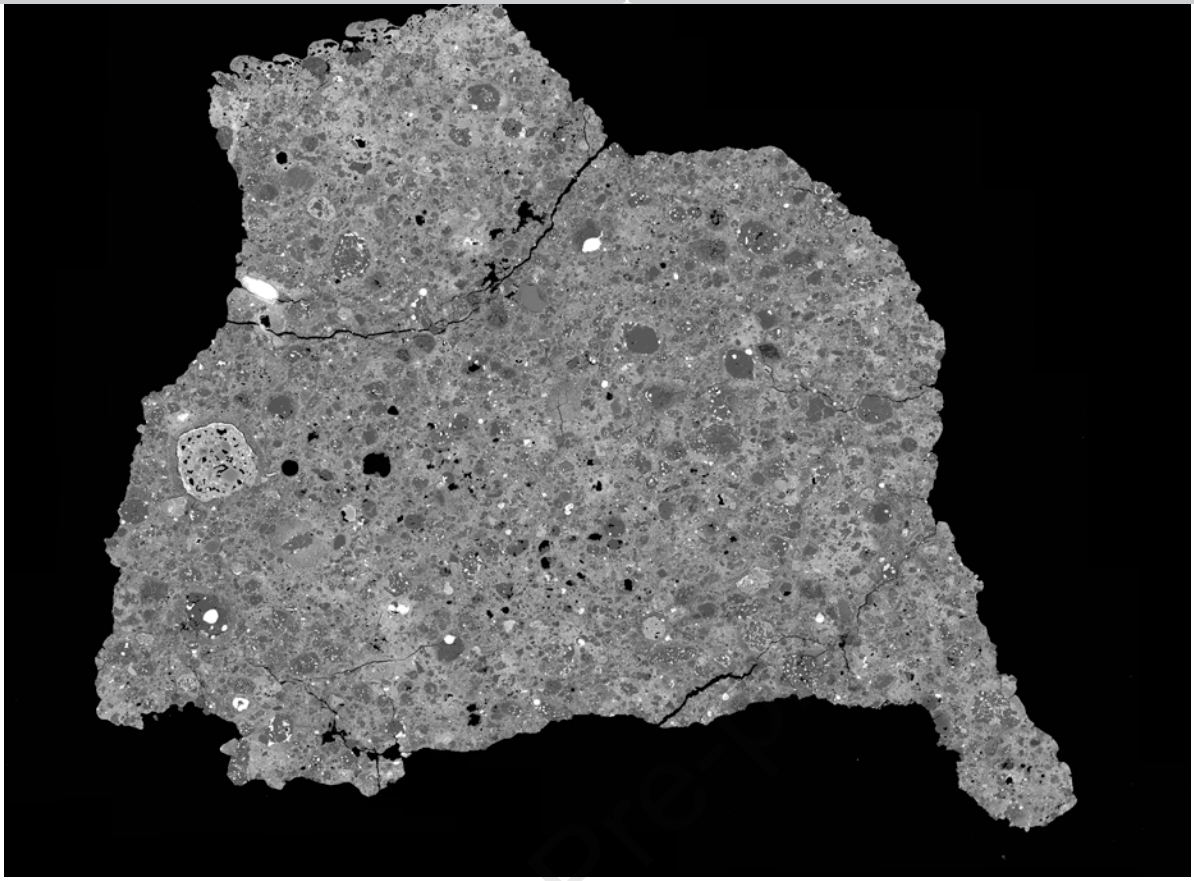

Fig. 1a

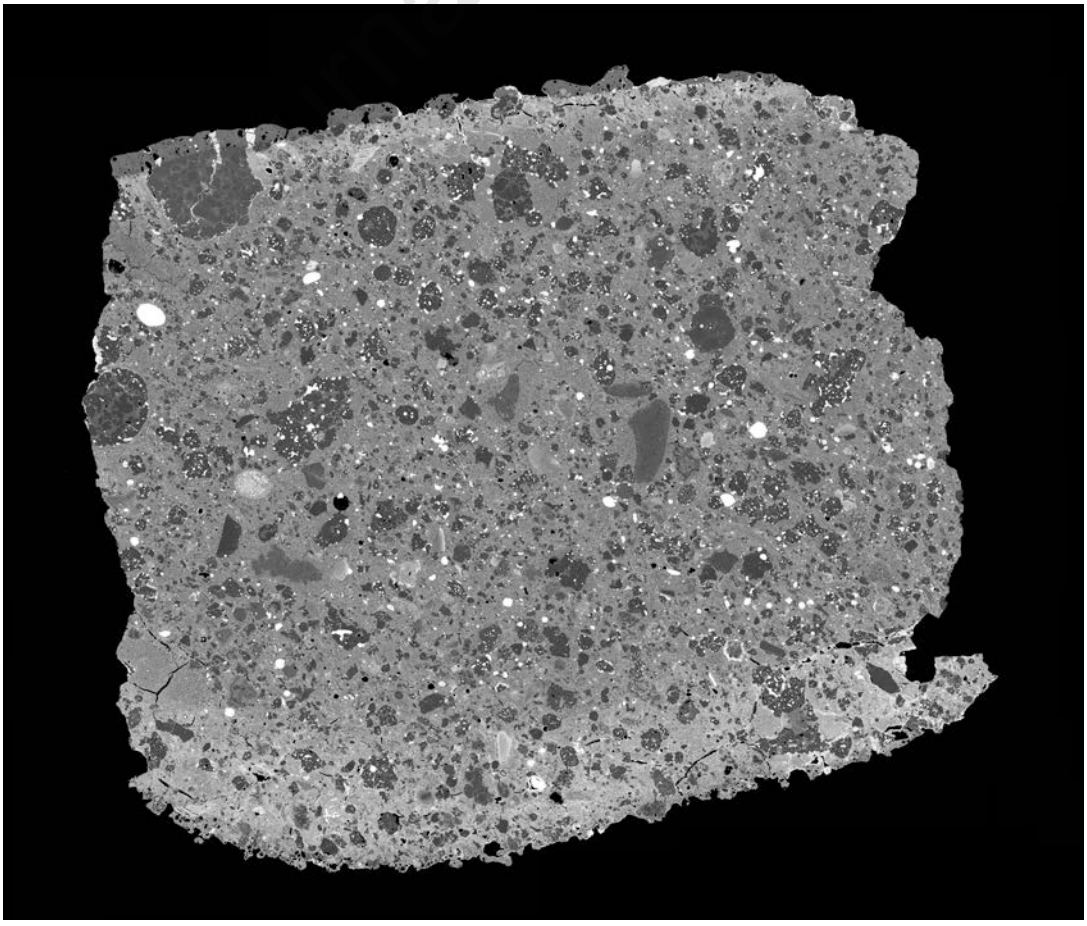

Fig. 1b

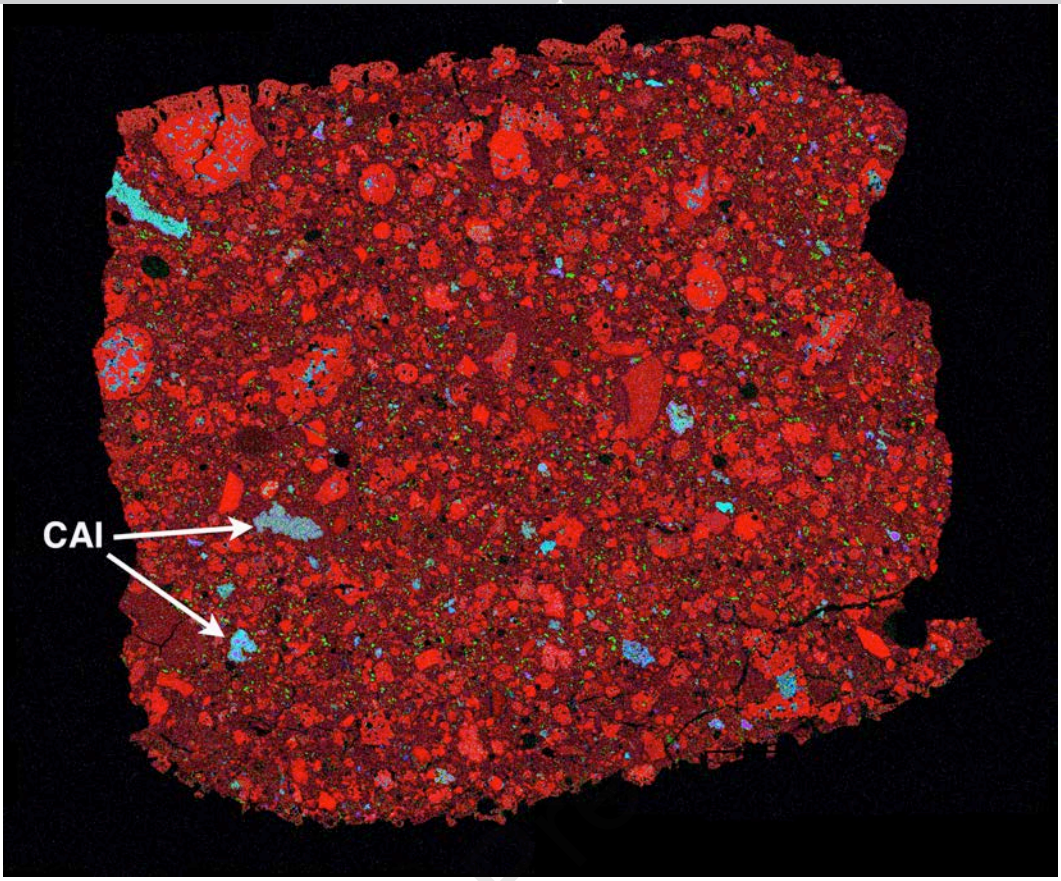

Fig. 1c

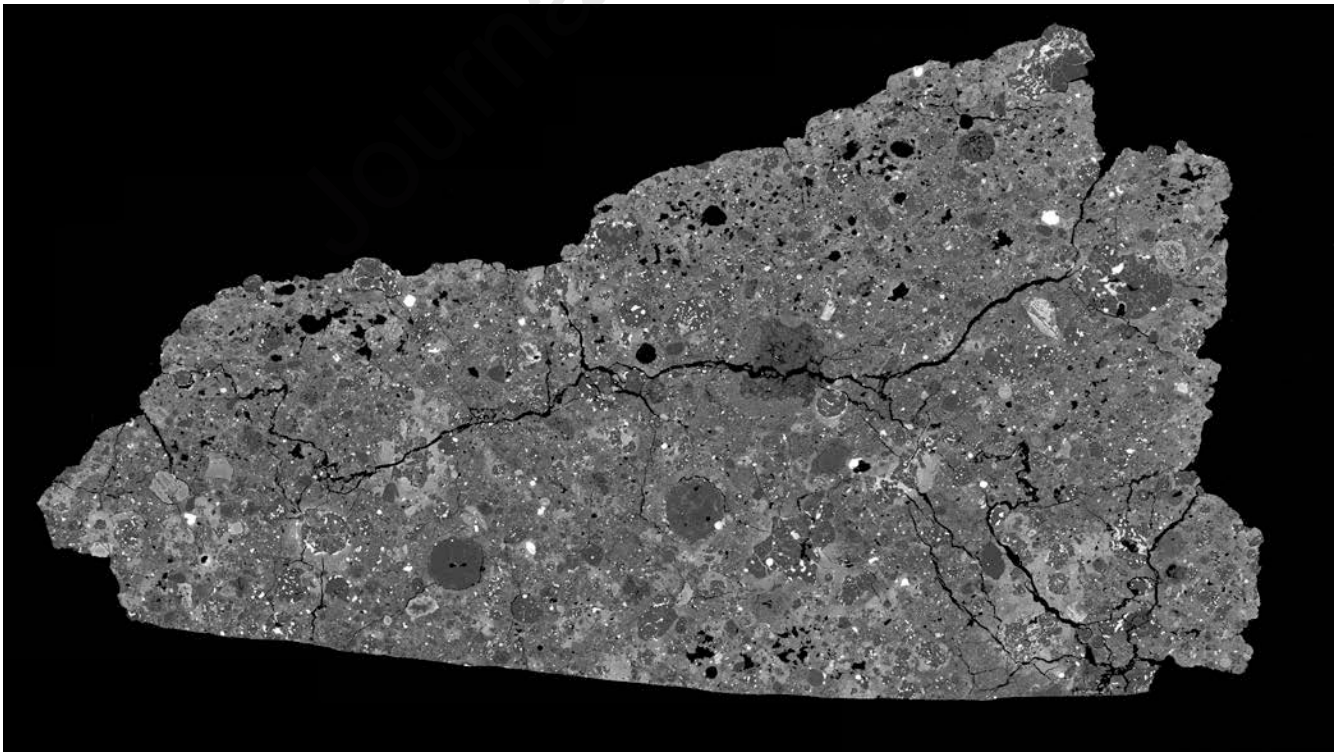

Fig. 1d

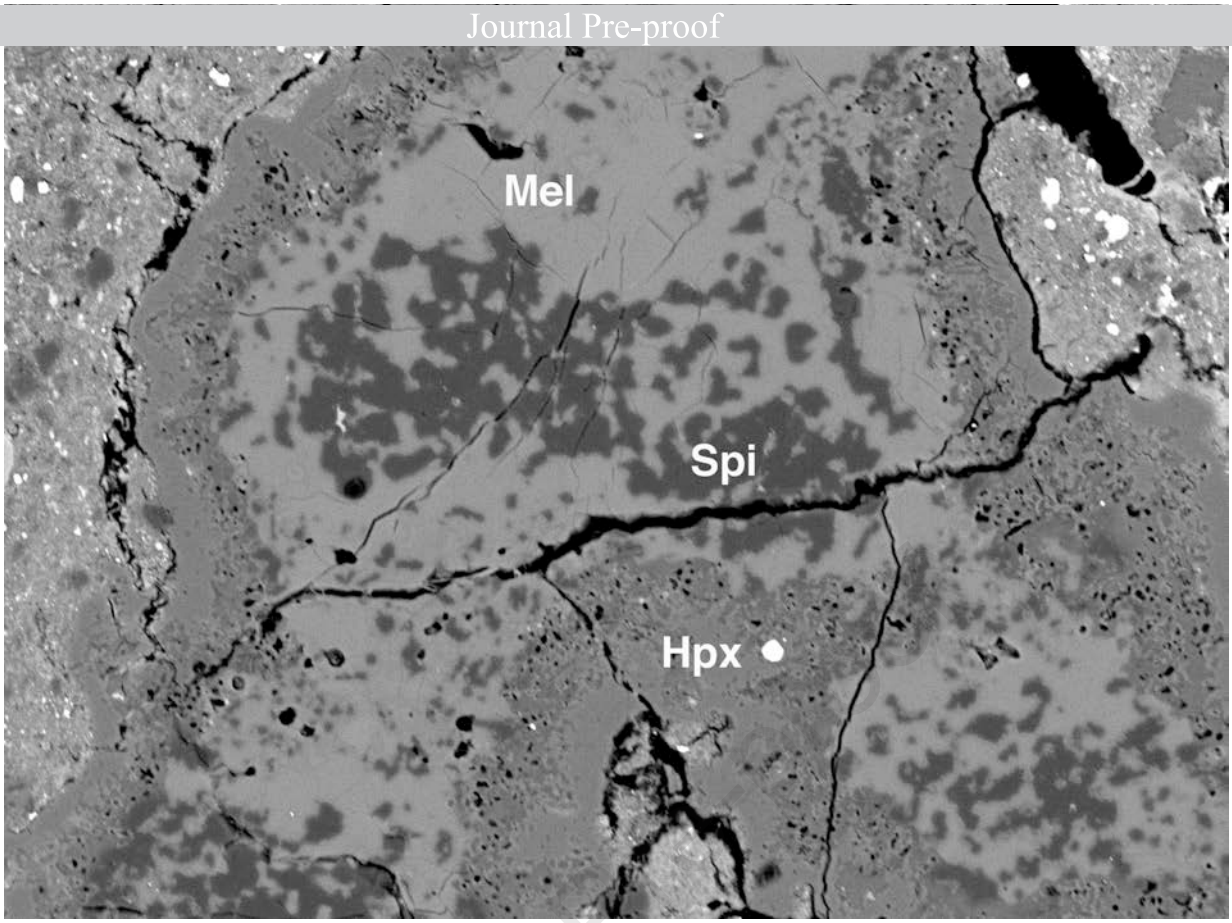

Fig. 2a

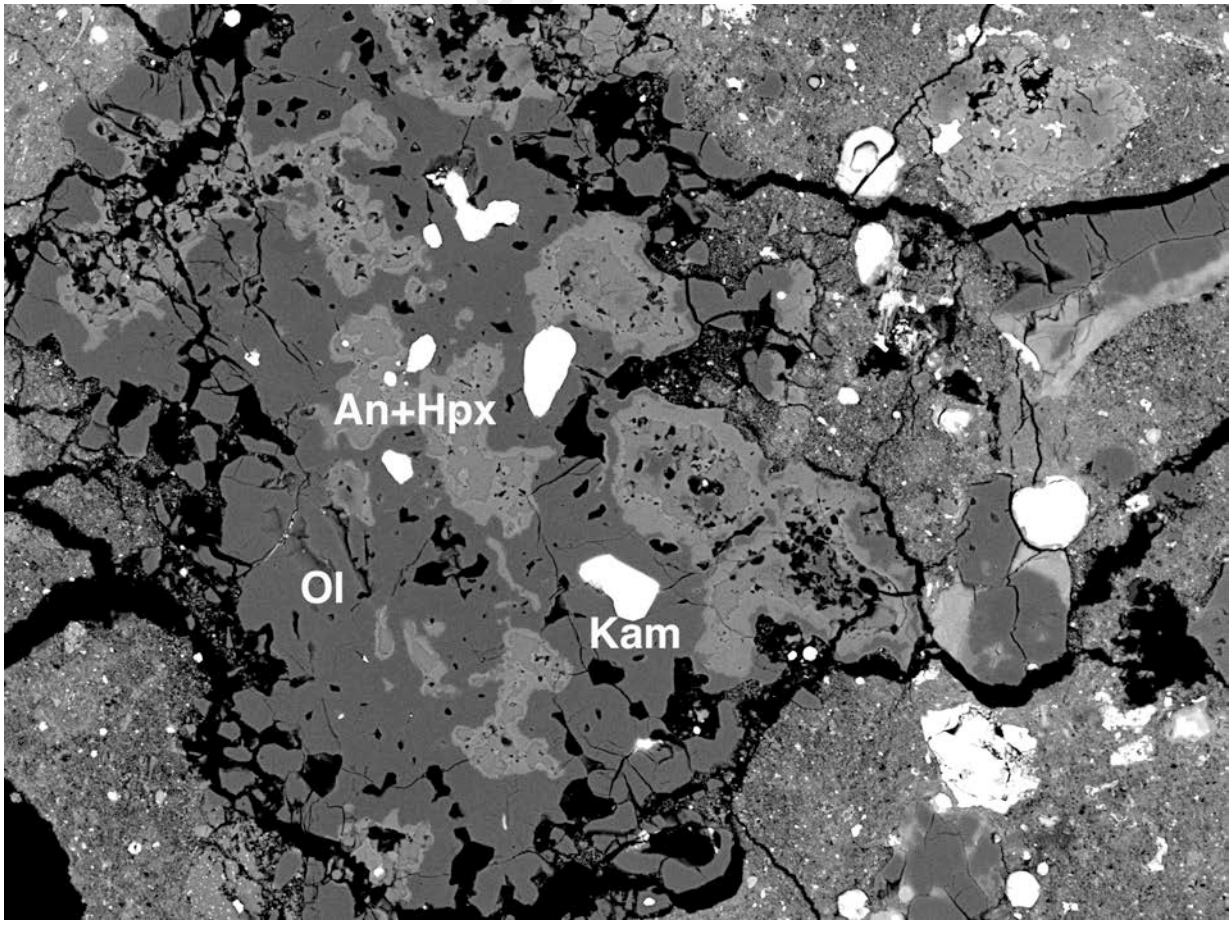

Fig. 2b

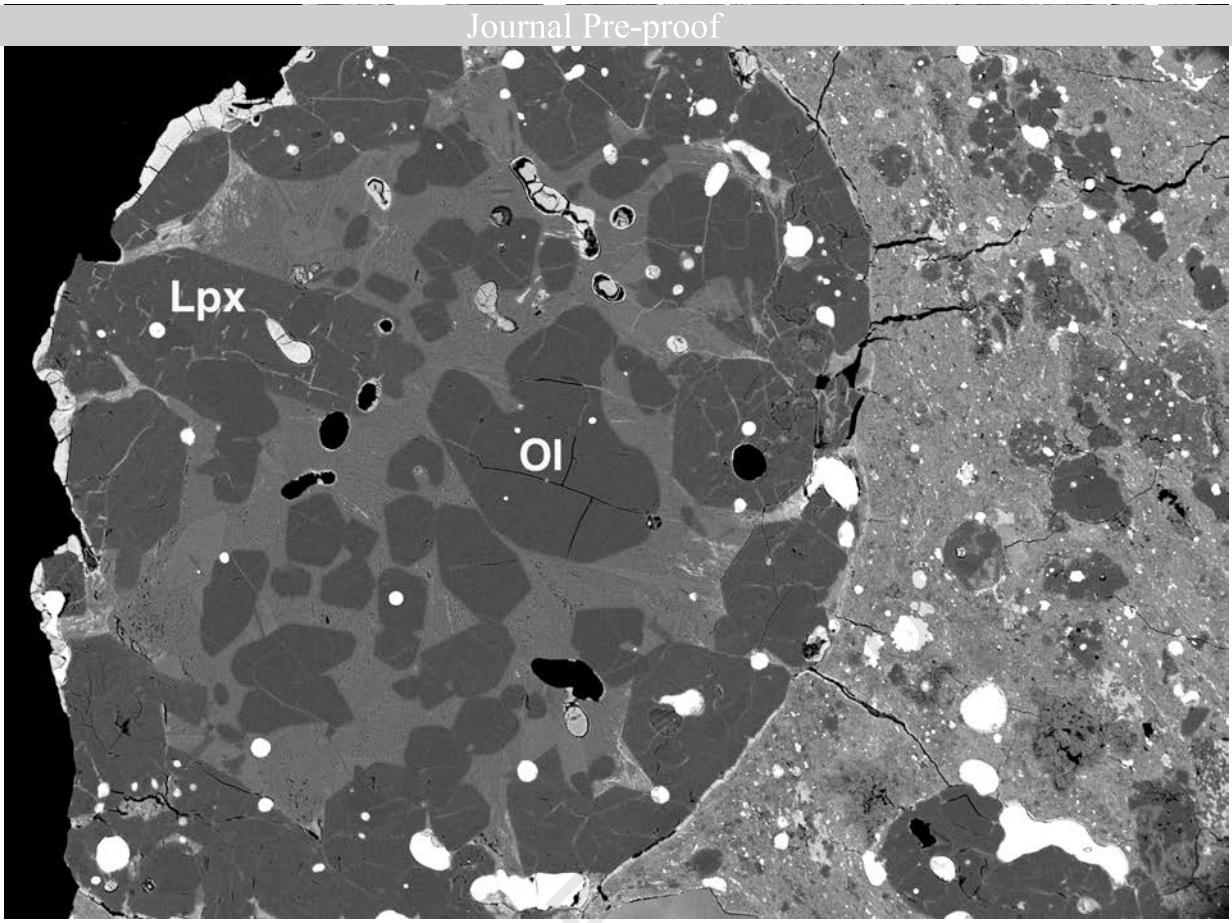

Fig. 2c

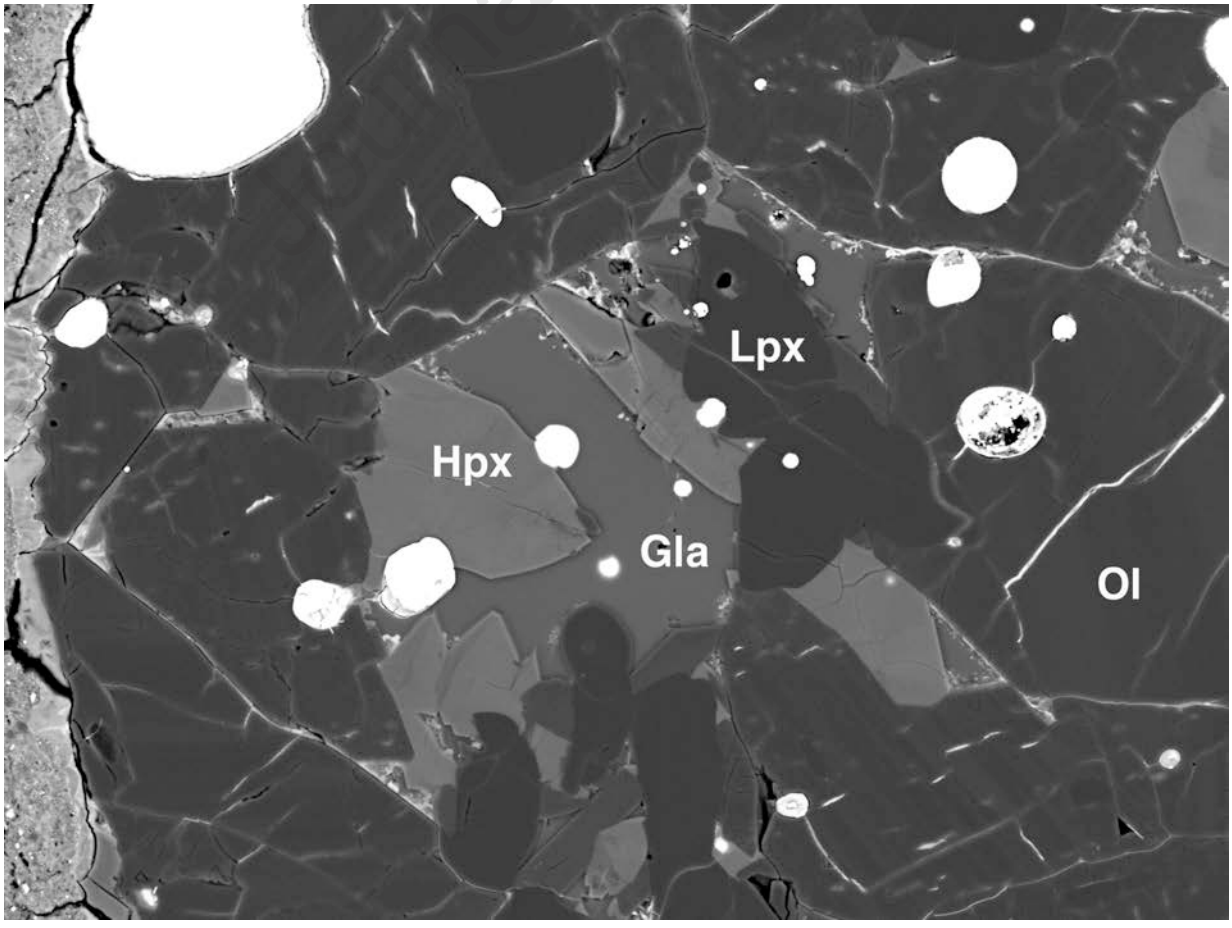

Fig. 2d

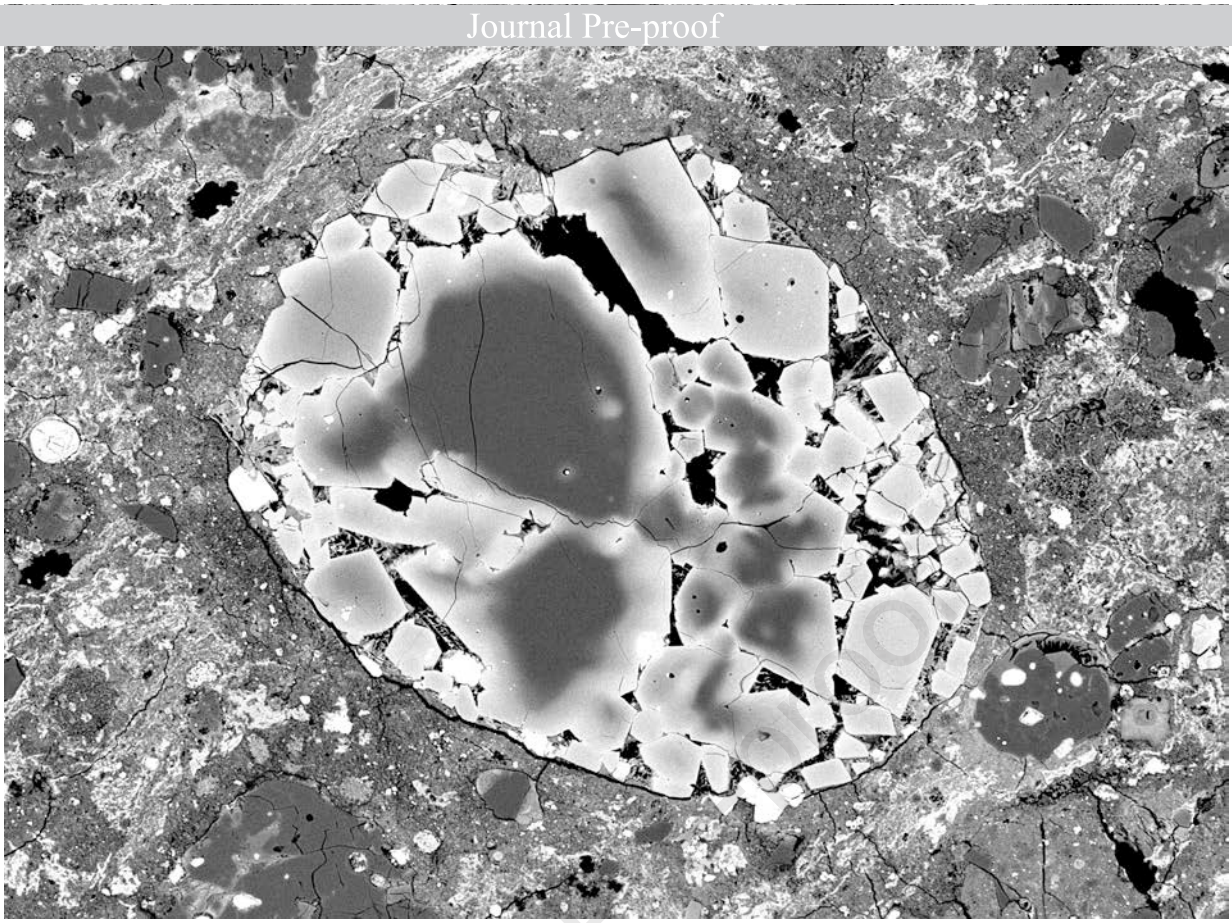

Fig. 2e

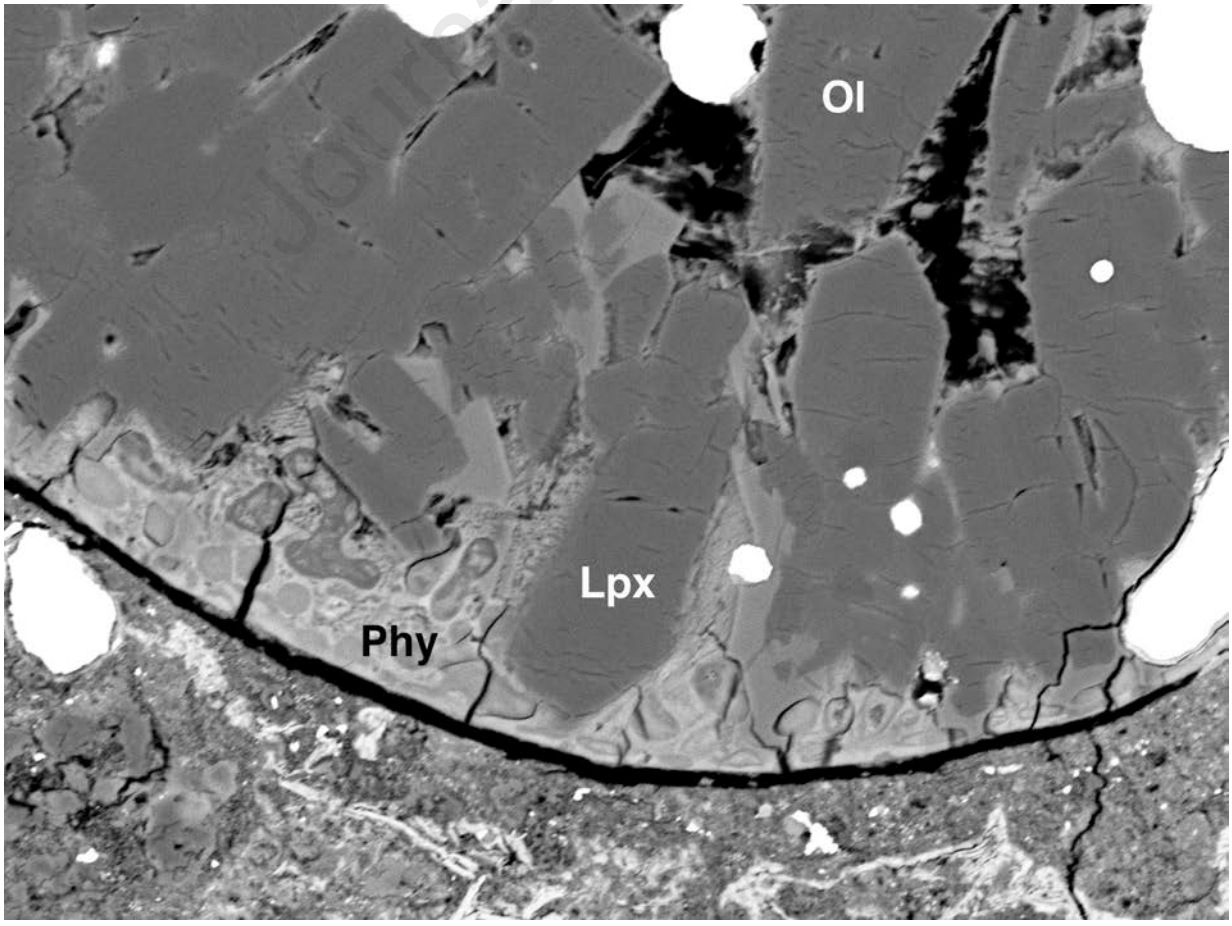

Fig. 2f

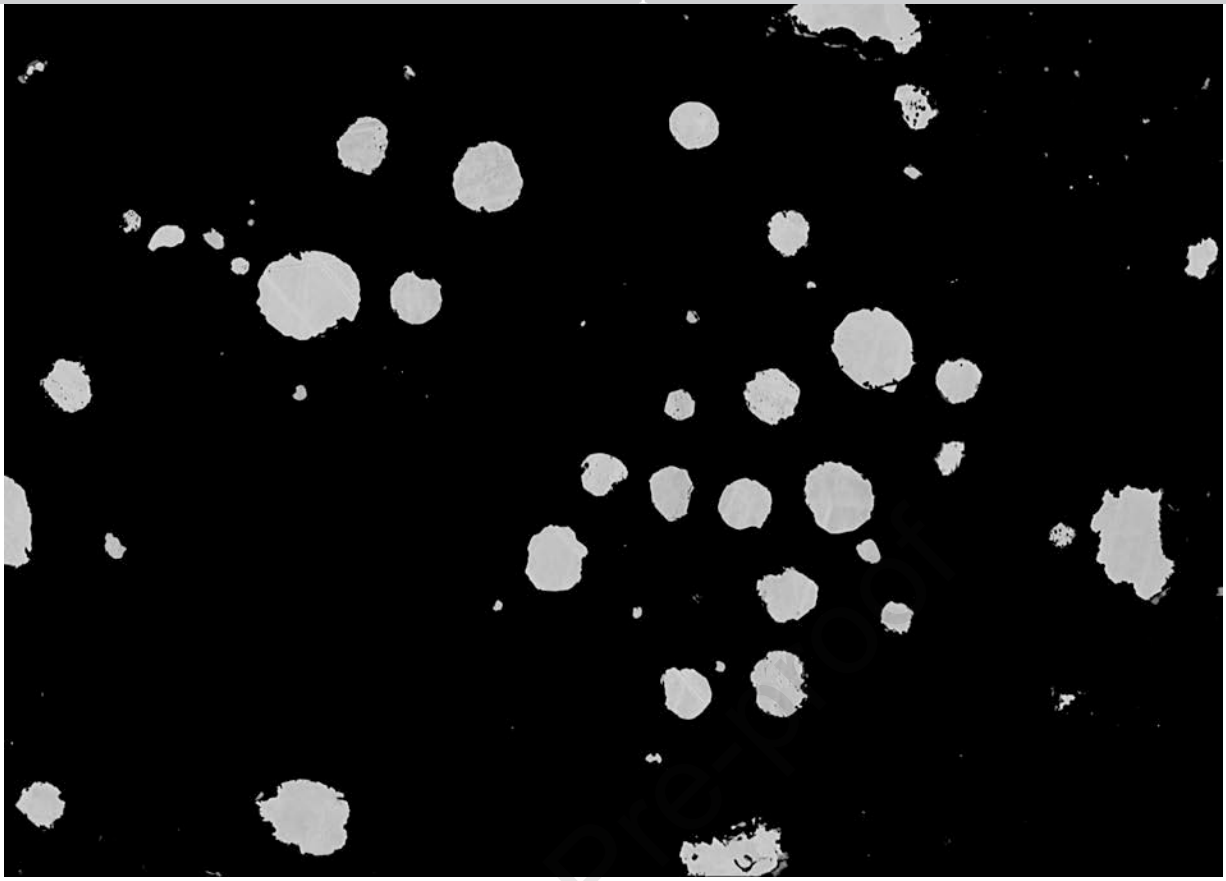

Fig. 2g

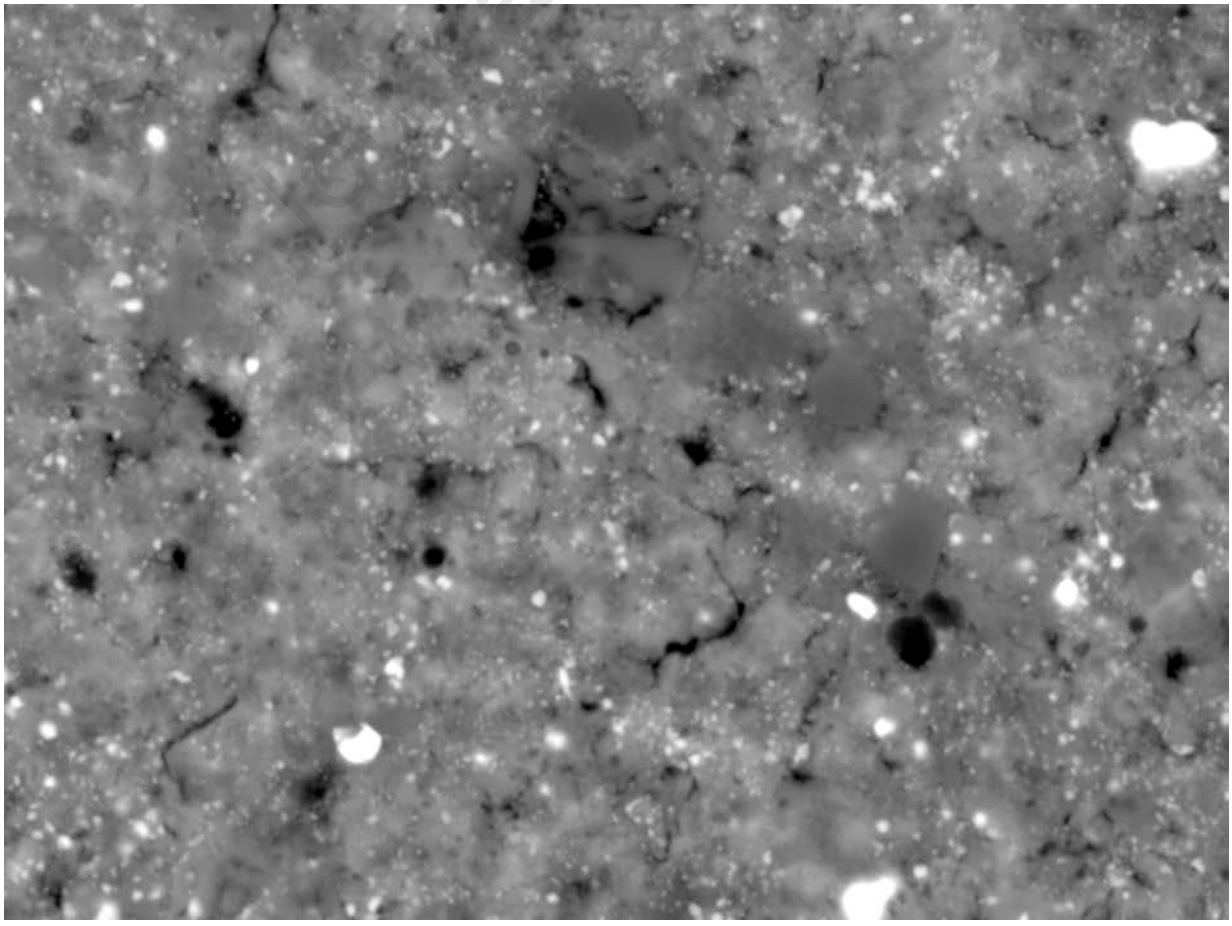

Fig. 2h

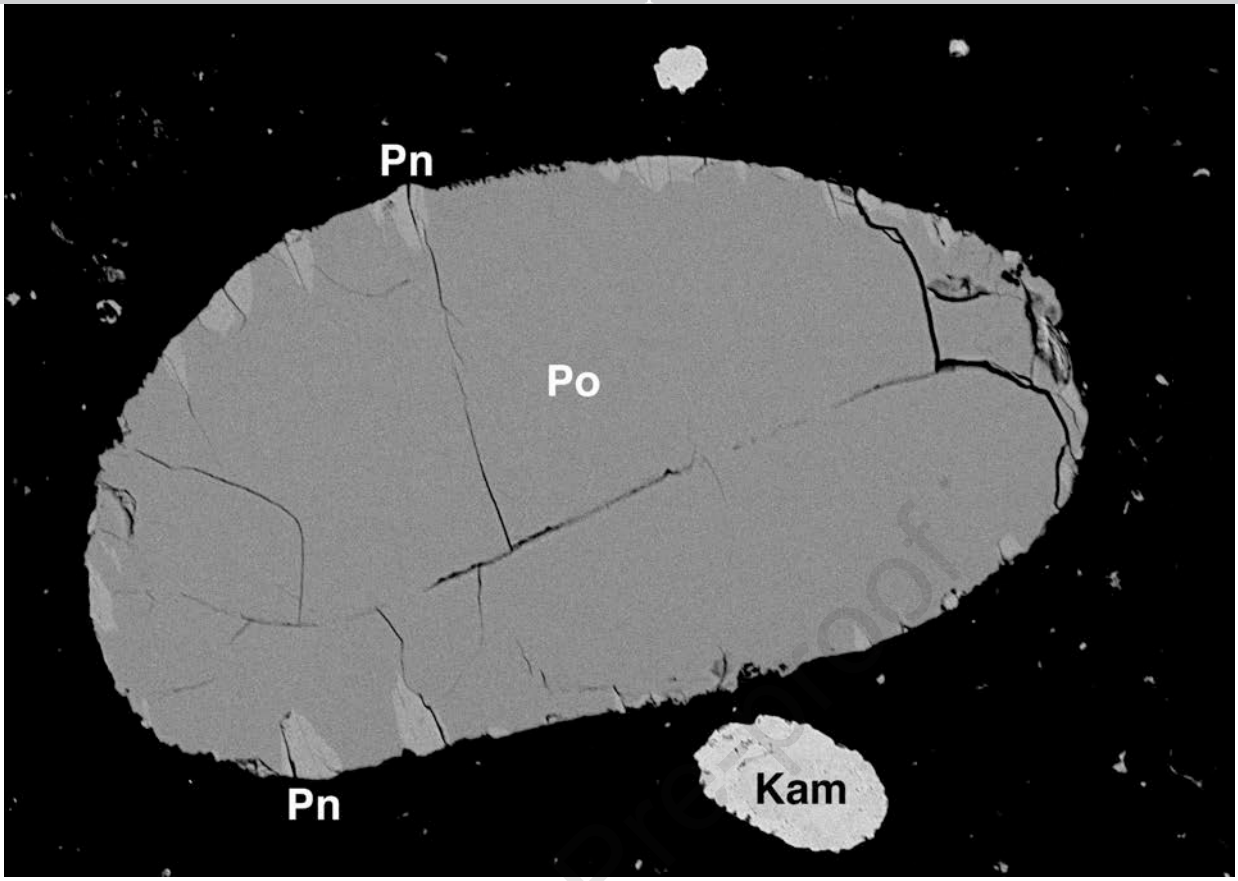

Fig. 2i

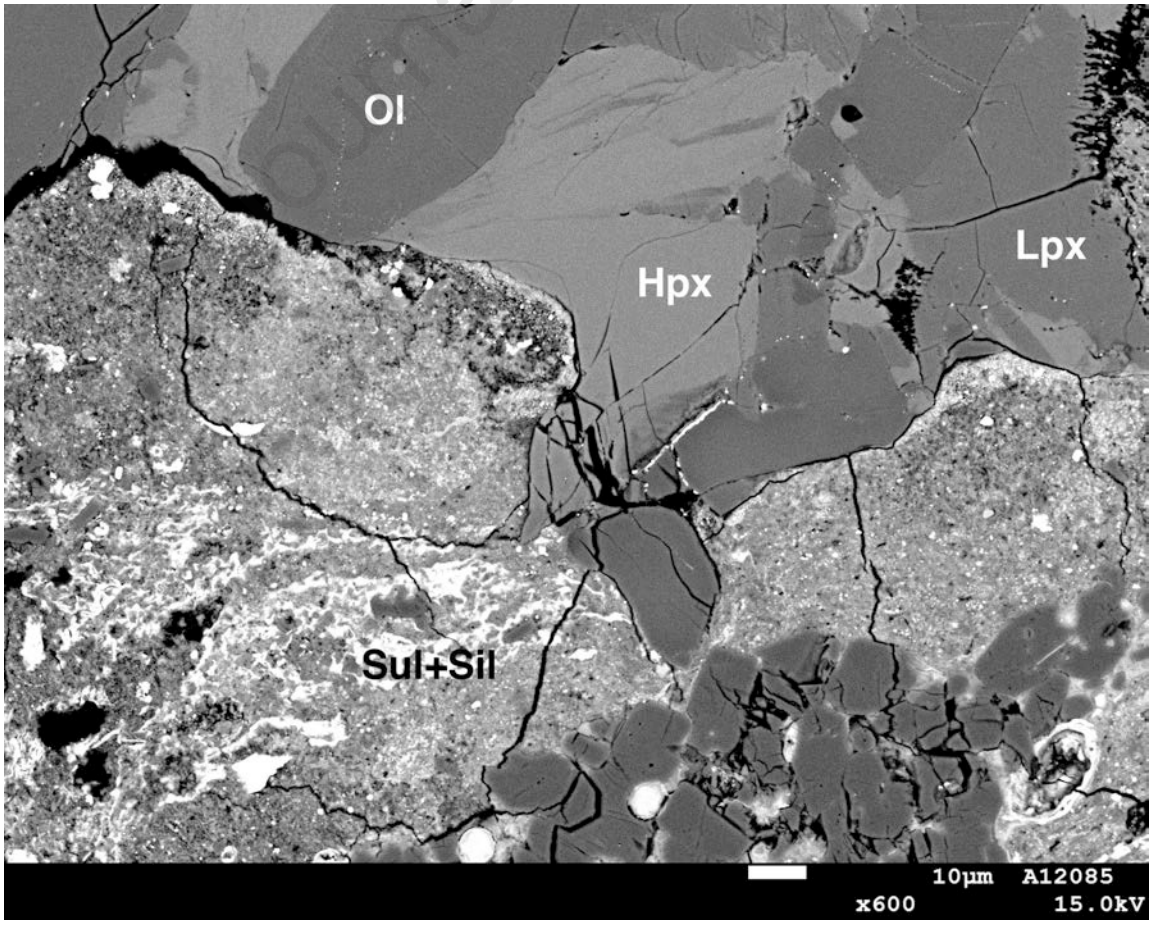

Fig. 2j

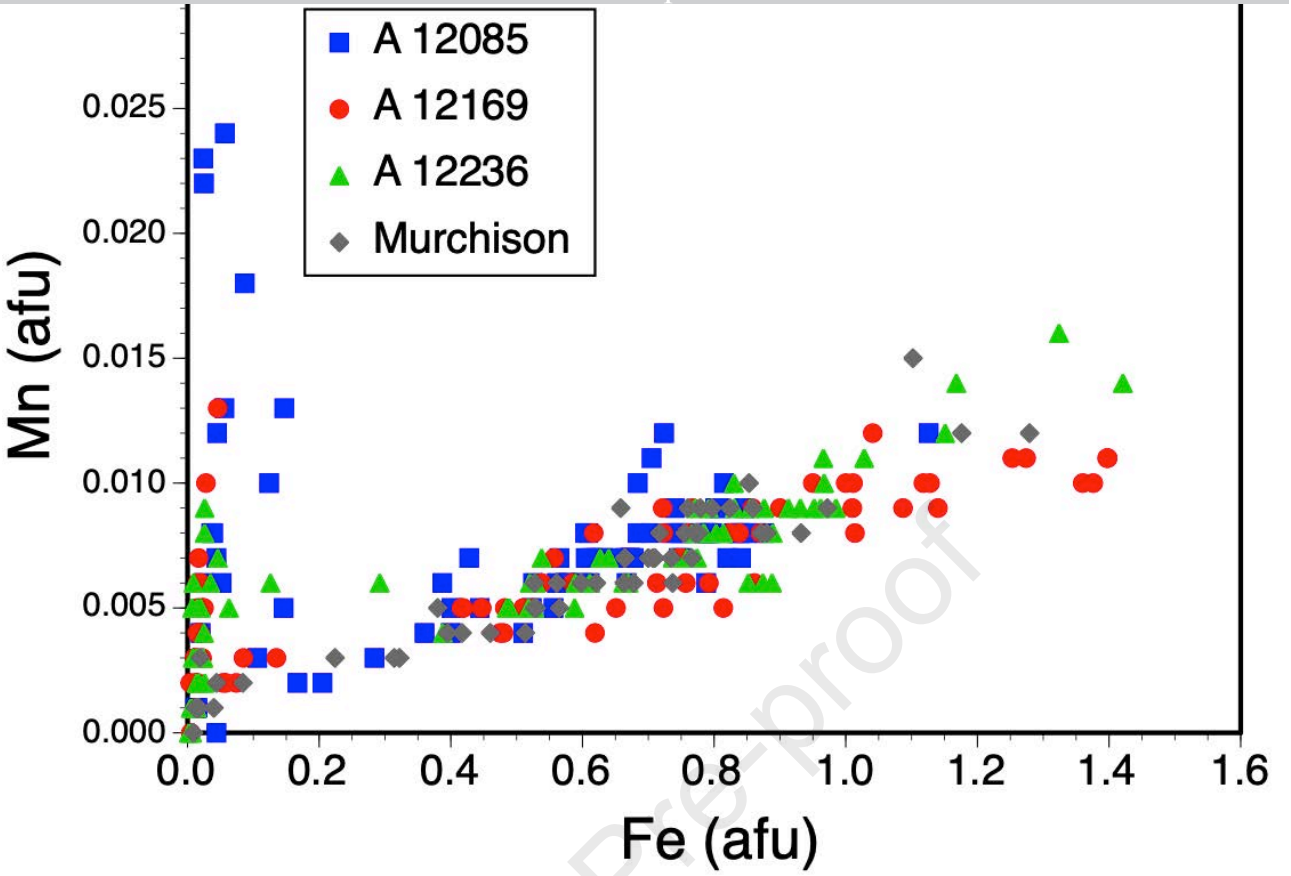

Fig. 3a

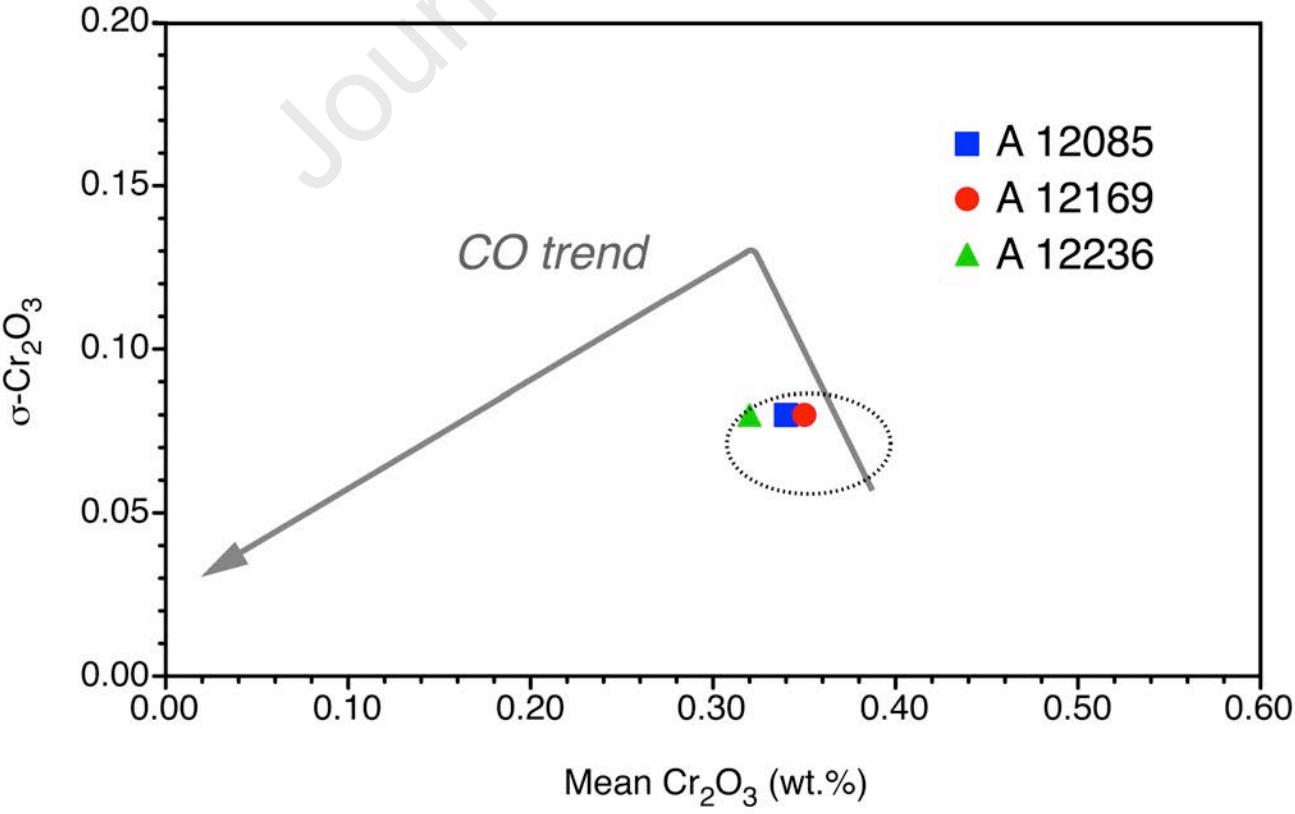

Fig. 3b

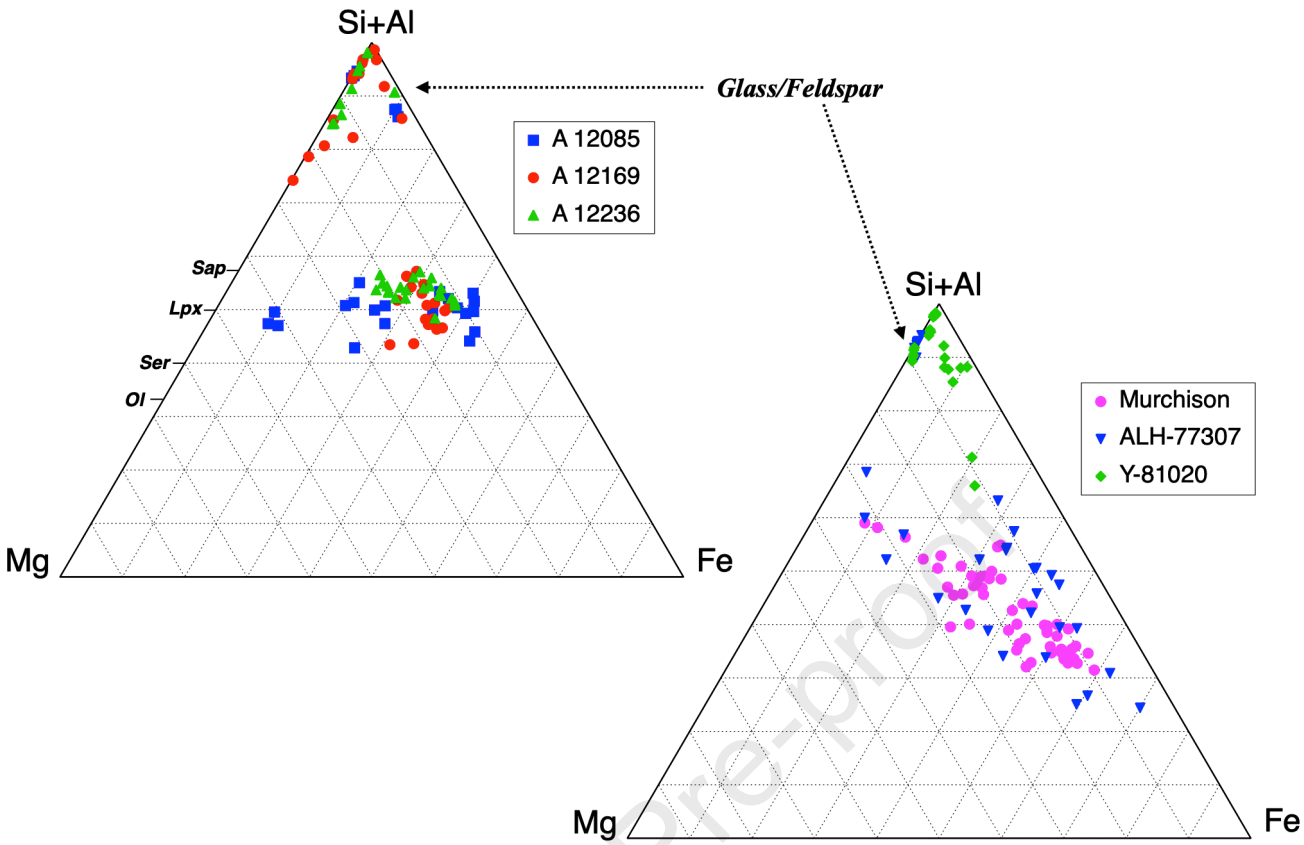

Fig. 4

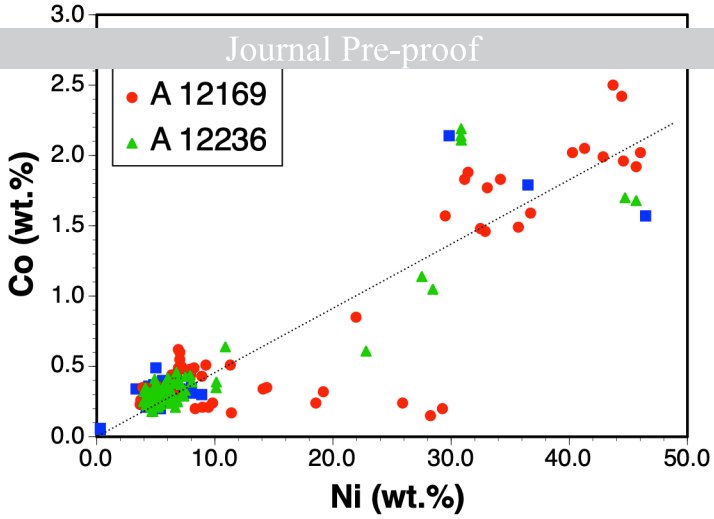

Fig. 5

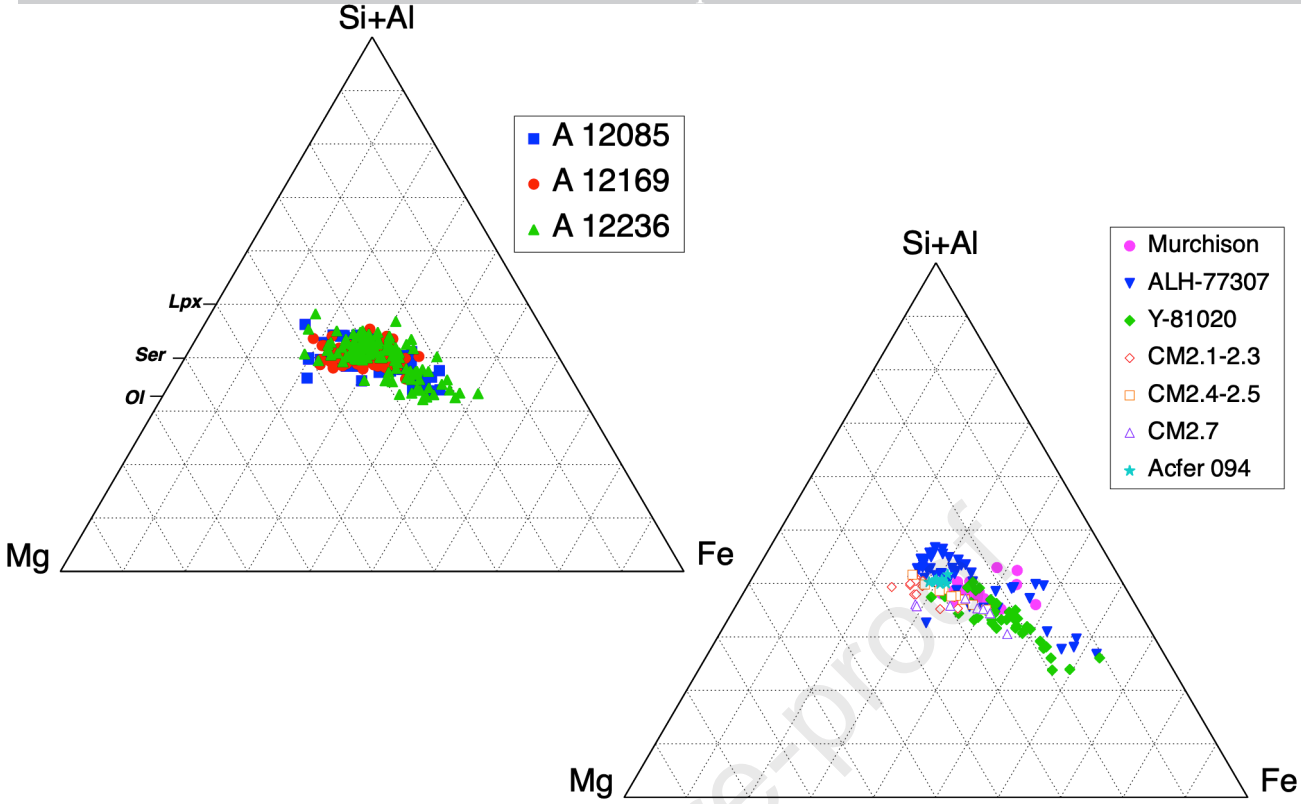

Fig. 6

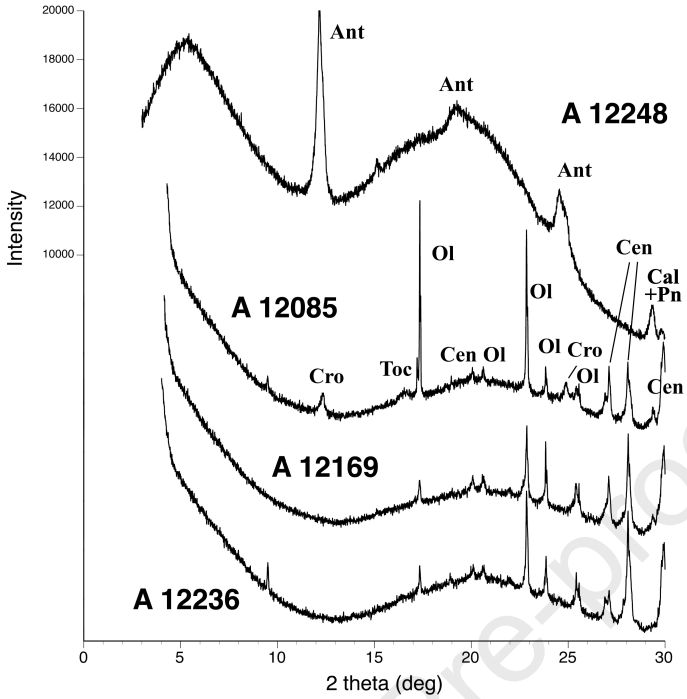

Fig. 7a

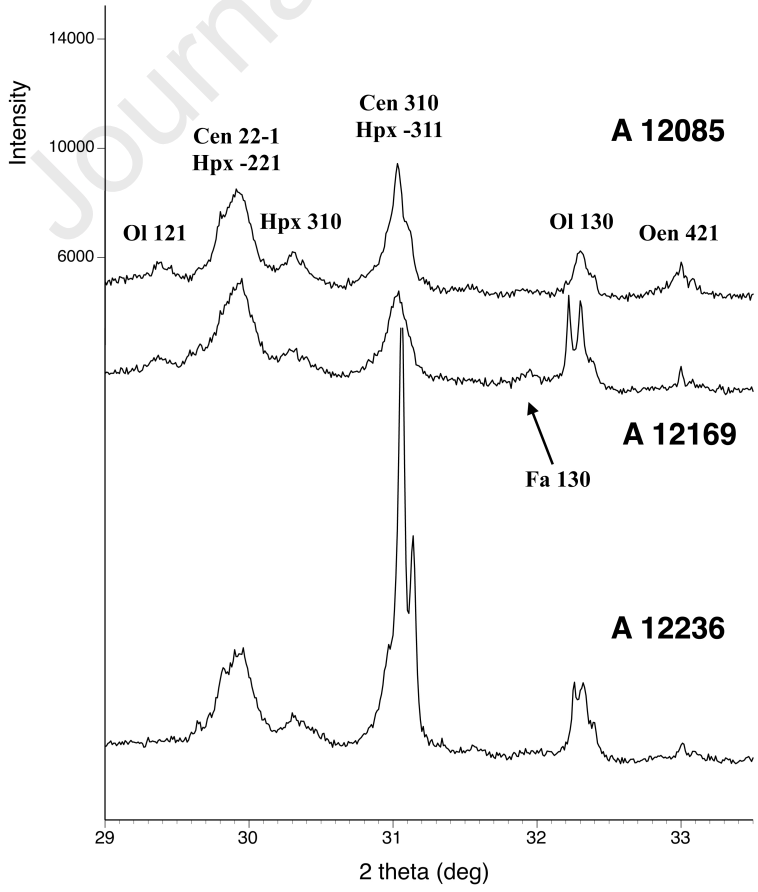

Fig. 7b

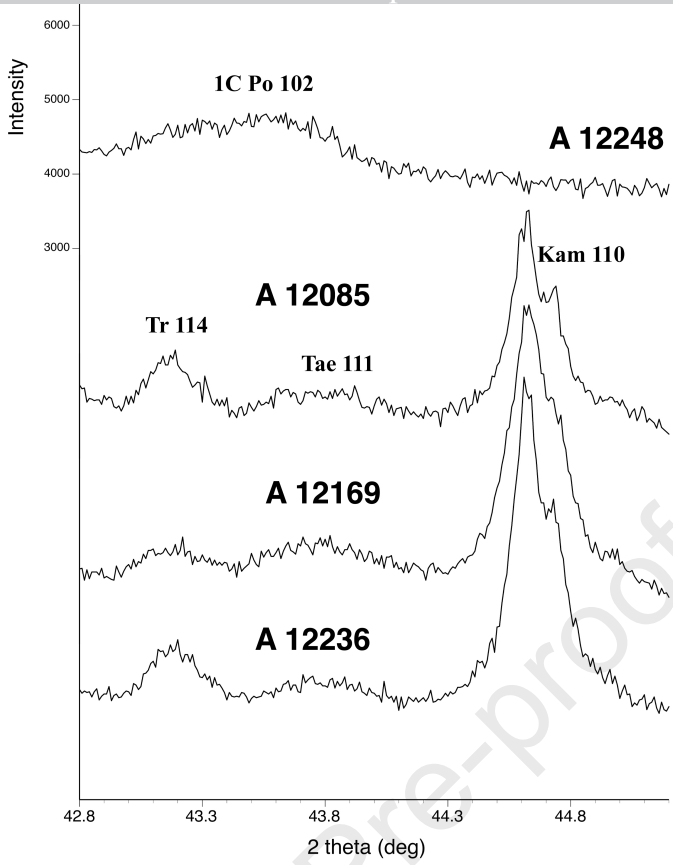

Fig. 7c

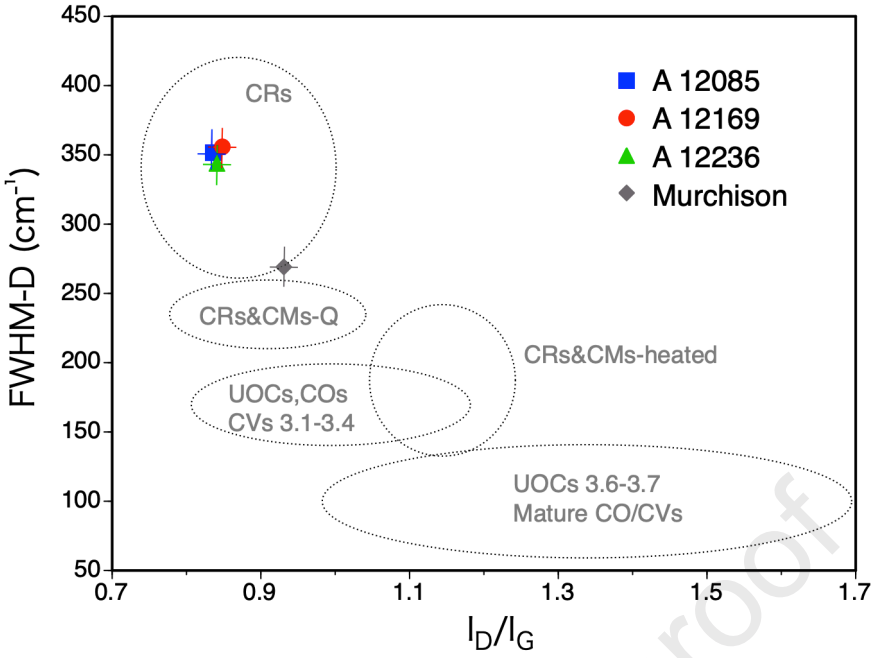

Fig. 8

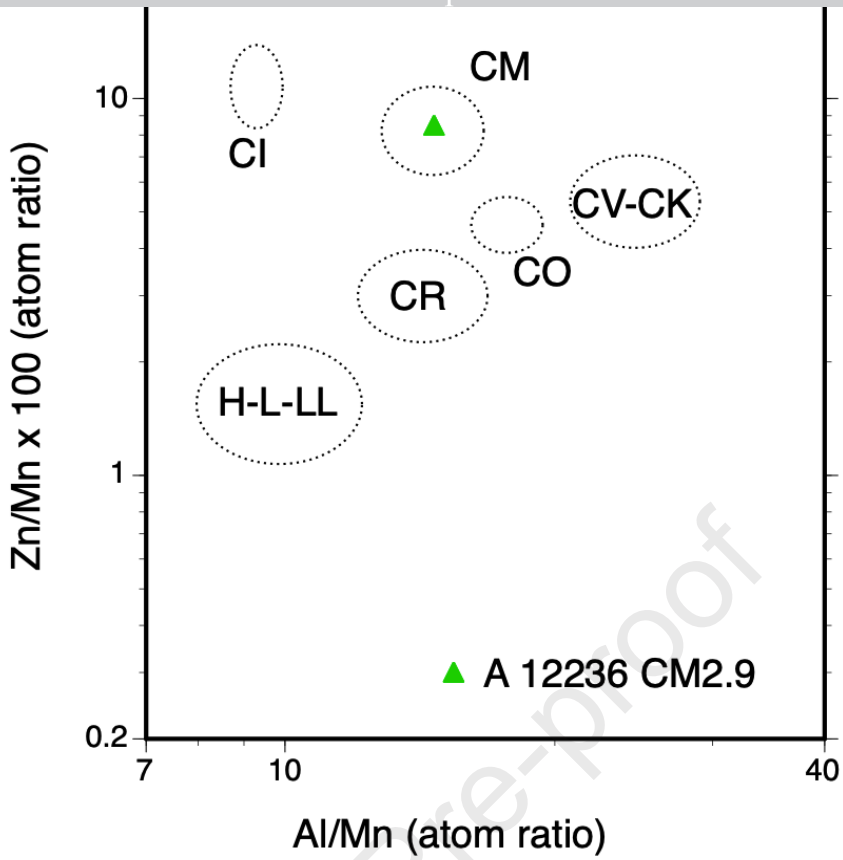

Fig. 9a

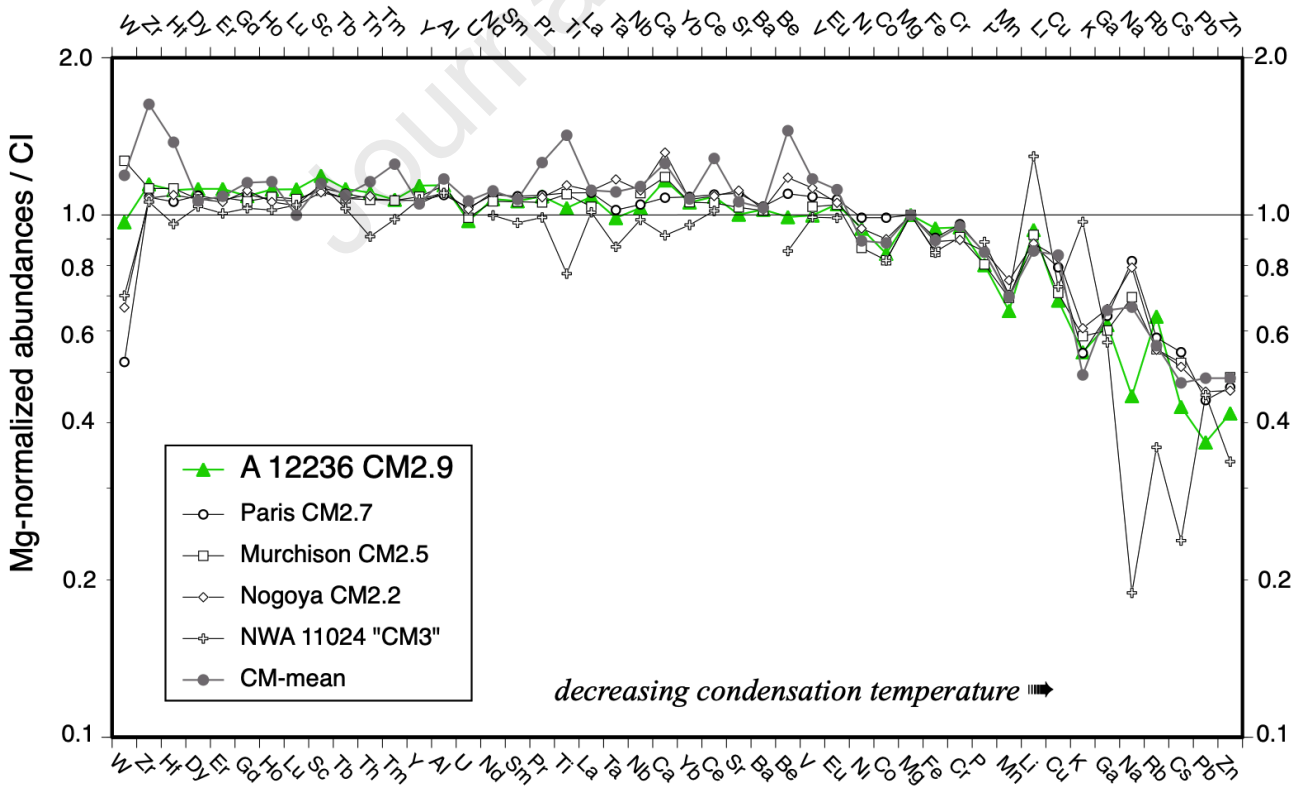

Fig. 9b